

## MIT Open Access Articles

*Biphilic Organophosphorus-Catalyzed Intramolecular C[<sub>sp2</sub>]-H Amination: Evidence for a Nitrenoid in Catalytic Cadogan Cyclizations*

The MIT Faculty has made this article openly available. **Please share** how this access benefits you. Your story matters.

**Citation:** Nykaza, Trevor et al. "Biphilic Organophosphorus-Catalyzed Intramolecular C[<sub>sp2</sub>]-H Amination: Evidence for a Nitrenoid in Catalytic Cadogan Cyclizations." *Journal of the American Chemical Society* 140, 8 (February 2018): 3103-3113 © 2018 American Chemical Society

**As Published:** <http://dx.doi.org/10.1021/jacs.7b13803>

**Publisher:** American Chemical Society (ACS)

**Persistent URL:** <https://hdl.handle.net/1721.1/123442>

**Version:** Author's final manuscript: final author's manuscript post peer review, without publisher's formatting or copy editing

**Terms of Use:** Article is made available in accordance with the publisher's policy and may be subject to US copyright law. Please refer to the publisher's site for terms of use.





Published in final edited form as:

*J Am Chem Soc.* 2018 February 28; 140(8): 3103–3113. doi:10.1021/jacs.7b13803.

## Biphilic Organophosphorus-Catalyzed Intramolecular C<sub>sp2</sub>-H Amination: Evidence for a Nitrenoid in Catalytic Cadogan Cyclizations

Trevor V. Nykaza<sup>†</sup>, Antonio Ramirez<sup>‡</sup>, Tyler S. Harrison<sup>†</sup>, Michael R. Luzung<sup>\*‡</sup>, and Alexander T. Radosevich<sup>\*†</sup>

<sup>†</sup>Department of Chemistry, Massachusetts Institute of Technology, Cambridge, Massachusetts 02139, United States

<sup>‡</sup>Chemical and Synthetic Development, Bristol-Myers Squibb Company, One Squibb Drive, New Brunswick, New Jersey 08903, United States

### Abstract

A small-ring phosphacycloalkane (1,2,2,3,4,4-hexamethylphosphetane, **3**) catalyzes intramolecular C–N bond forming heterocyclization of *o*-nitrobiaryl and –styrenyl derivatives in the presence of a hydrosilane terminal reductant. The method provides scalable access to diverse carbazole and indole compounds under operationally trivial homogeneous organocatalytic conditions, as demonstrated by 17 examples conducted on one-gram scale. In situ NMR reaction monitoring studies support a mechanism involving catalytic P<sup>III</sup>/P<sup>V</sup>=O cycling, where tricoordinate phosphorus compound **3** represents the catalytic resting state. For the catalytic conversion of *o*-nitrobiphenyl to carbazole, the kinetic reaction order was determined for phosphetane catalyst **3** (first order), substrate (first order), and phenylsilane (zeroth order). For differentially 5-substituted 2-nitrobiphenyls, the transformation is accelerated by electron-withdrawing substituents (Hammett factor  $\rho = +1.5$ ), consistent with the accrual of negative charge on the nitro substrate in the rate-determining step. DFT modeling of the turnover-limiting deoxygenation event implicates a rate-determining (3+1) cheletropic addition between the phosphetane catalyst **3** and 2-nitrobiphenyl substrate to form an unobserved pentacoordinate spiro-bicyclic dioxazaphosphetane, which decomposes via (2+2) cycloreversion giving one equivalent of phosphetane *P*-oxide **3**•[O] and 2-nitrosobiphenyl. Experimental and computational investigations into the C–N bond forming event suggest the involvement of an oxazaphosphirane (2+1) adduct between **3** and 2-nitrosobiphenyl, which evolves through loss of phosphetane *P*-oxide **3**•[O] to give the observed carbazole product via C–H insertion in a nitrene-like fashion.

### Table of Contents artwork

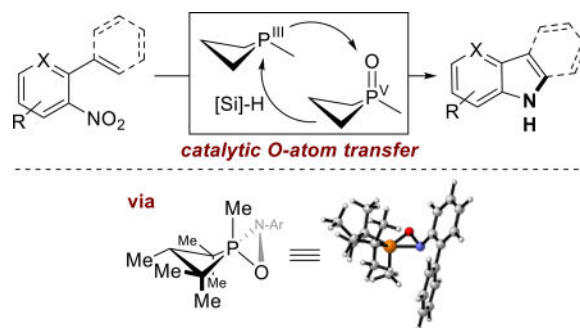
\*Corresponding Authors. michael.luzung@bms.com, radosevich@mit.edu.

#### ASSOCIATED CONTENT

Supporting Information

Synthetic procedures; <sup>1</sup>H, <sup>13</sup>C, <sup>15</sup>N and <sup>31</sup>P NMR spectra; kinetics data; computational details and Cartesian coordinates

The authors declare no competing financial interests.



## 1. Introduction

Nitrogen containing heterocyclic compounds, such as carbazoles and indoles, are important synthetic targets due to their prevalence in bioactive natural metabolites and pharmaceuticals,<sup>1</sup> as well as their application in functional optoelectronic materials.<sup>2</sup> Accordingly, numerous synthetic methods exist for their production. Among the methods to synthesize carbazoles<sup>1a,3</sup> and indoles,<sup>4</sup> those involving direct cyclization via C–H amination are attractive.<sup>5</sup> The carbazole-/indole-forming method of Sundberg, involving heterocyclization by thermolysis or photolysis of *o*-azidonitrobiaryls and *o*-azidostyrenes and proceeding via an aryl nitrene C–H insertion pathway,<sup>6</sup> exemplifies the efficiency of this bond construction (Figure 1A). Transition metal catalysts have more recently been found to bring about similar transformations of such azide substrates under milder thermal conditions,<sup>7</sup> although the inherent hazards associated with the preparation and handling of azide containing intermediates represent a practical constraint for such protocols on process synthesis scales.<sup>8</sup>

By way of complement, Cadogan has extensively documented that qualitatively similar azacyclizations can be driven by phosphine-mediated exhaustive deoxygenation of *o*-functionalized nitrobenzene derivatives (Figure 1A).<sup>9</sup> Chief advantages of this chemistry comprise the ease with which the aryl nitro moiety is installed and transformed in synthesis,<sup>10</sup> including its orthogonality with respect to many transition metal catalyzed chemistries. In common practice, Cadogan transformations employ superstoichiometric amounts of phosphorus-based reagents at elevated temperatures (typically neat refluxing triethylphosphite), although milder conditions<sup>11</sup> or alternative stoichiometric reagents<sup>12</sup> have been applied in some cases. The process mass intensity and inherent inefficiencies of the stoichiometric Cadogan method have been persistent drawbacks that have limited its use on large synthetic scales.<sup>13</sup>

Catalytic variants of Cadogan-like reductive cyclizations of nitroarenes have been developed that in part address these challenges. For instance, numerous reports have described the use of palladium catalysis in conjunction with CO as a terminal reductant to achieve intramolecular heterocyclization of nitro substrates (Figure 1B).<sup>14</sup> Despite the laboratory scale appeal of these synthetically useful methods, the difficulty of purging Lewis acidic metal catalysts from the nitrogen-rich products of cyclization and the use of pressurized carbon monoxide as a terminal reductant (which triggers the need for specialized reactors

and safety protocols, especially in kilo lab and pilot plant settings) increase the operational complexity of synthetic routes in which these methods are employed. A notable exception in this latter regard is a recent report from Driver,<sup>15</sup> who has developed an iron-hydride catalyzed synthesis of carbazoles and related derivatives in which the terminal reductant is a relatively innocuous liquid hydrosilane.

Our group has been pursuing a program aimed at developing designer main group compounds as biphilic<sup>16</sup> organocatalysts in organic synthesis.<sup>17</sup> In this vein, we recently reported that a simple trialkylphosphine catalyst containing a core four-membered ring, in combination with phenylsilane as a terminal reductant, provided a competent system for the catalytic reductive N–N bond forming heterocyclization of *o*-nitrobenzaldehydes giving 2*H*-indazoles.<sup>18</sup> In this chemistry, the phosphacyclic catalyst promotes reductive *O*-atom transfer from the nitroarene substrates by cycling in the P<sup>III</sup>/P<sup>V</sup>=O catalytic couple. The varied catalytic chemistry of phosphine oxides is experiencing rapid expansion,<sup>19</sup> and the potential of P<sup>III</sup>/P<sup>V</sup>=O redox methods<sup>20</sup> in particular to favorably impact the process intensity of otherwise stoichiometric phosphorus-mediated transformations has been specifically noted.<sup>21</sup>

Based on this precedent, we wished to ascertain whether the reactive intermediates generated from nitroarenes under P<sup>III</sup>/P<sup>V</sup>=O catalytic conditions would be applicable to the construction of C–N bonds in an intramolecular Cadogan-like manner (Figure 1C). In this study, we report the discovery, development, and mechanistic evaluation of such a new biphilic organophosphorus-catalyzed method for carbazole and indole synthesis. The key features of the system we describe here include: (1) a practical, scalable, and operationally robust organophosphorus-catalyzed protocol for C–H functionalizing Cadogan azacyclizations that greatly simplifies product isolation for this class of reactions, (2) a combined experimental and computational assessment of the reaction mechanism for nitro deoxygenation and subsequent C–N bond formation that provides evidence for the controlling role of *P*-based biphilic reactivity in these catalytic Cadogan cyclizations, and (3) spectroscopic evidence for a heretofore unobserved adduct of a tricoordinate phosphorus compound and a nitrosoarene that we propose serves as the immediate precursor to C–H amination in the catalytic transformation. Taken together, these findings enrich fundamental understanding of the intermediate speciation in phosphine/nitroarene reactions and advance the biphilic reactivity of phosphinanes as generalized platforms for catalytic reductive *O*-atom transfer operating in the P<sup>III</sup>/P<sup>V</sup>=O redox manifold.

## 2. Results

### 2.1 Optimization of Reaction Conditions

Consistent with observations made during the discovery of our previously reported catalytic N–N bond forming Cadogan indazolation, reaction of *o*-nitrobiphenyl **1** with a substoichiometric amount (15 mol%) of methyl phosphinane *P*-oxide **3**•[O] and phenylsilane (2 equiv) produced carbazole product **2** with a GC yield of 84% after 16 h at 100 °C (Table 1, entry 1). Alteration of the exocyclic *P*-substituent was found to lower the catalytic reactivity; significantly lower yields were obtained under otherwise identical conditions for *P*-phenyl phosphinane **4**•[O] (entry 2) and *P*-pyrrolidino phosphinane **5**•[O] (entry 3).

Control experiments demonstrate that the reaction does not occur when either the precatalyst **3**•[O] (entry 4) or phenylsilane terminal reductant (entry 5) are omitted. Furthermore, the use of 15 mol% of P<sup>III</sup> phosphetane **3** as catalyst in the presence of phenylsilane reductant produced a qualitatively similar amount of carbazole **2** (entry 6) as when **3**•[O] is employed (entry 1), consistent with notion of catalysis involving cycling between P<sup>III</sup>/P<sup>V</sup>=O species.

The four-membered phosphacycle of catalysts **3**/**3**•[O] appears crucial for efficient carbazole formation. Five-membered ring containing phospholane-based precatalysts (**6**•[O] and **7**•[O], entries 7, 8), which have previously been applied to catalytic P<sup>III</sup>/P<sup>V</sup>=O Wittig<sup>20a,c,d,g-i</sup> and Appel<sup>20b</sup> reactions, gave low yield of carbazole **2**. Moreover, acyclic phosphine oxides (**8**•[O], **9**•[O], and **10**•[O], entries 9–11) exhibited poor catalytic reactivity.

The catalytic reaction is tolerant of varied reaction solvents, and further optimization studies converged on conditions using 20 mol% of **3**•[O] and 2 equiv of phenylsilane at 120 °C in *n*-butyl acetate, which gave excellent conversion to carbazole **2** (entry 12). A practical advantage of these conditions and the use of the low-volatility, process-scalable *n*-butyl acetate solvent<sup>22</sup> is that carbazole product **2** precipitates from the homogeneous catalytic reaction mixture upon cooling and can be collected in >98% purity (HPLC) by filtration in a straightforward fashion.

## 2.2 Reaction Scope

**2.2.1 Synthesis of carbazoles and related heterocycles**—An investigation of the scope of the catalytic carbazole synthesis was undertaken, with results collected in Table 2. In view of the procedural simplicity of the catalytic protocol, we elected to conduct all of these examples on one-gram scale; the products reported in Table 2 were obtained in excellent purity by simple filtration and washing. In these experiments, no special precautions were employed to exclude air or moisture from the reaction; all reagents and solvents were commercial grade and charged to the reaction vessel under ambient atmosphere. In this manner, a variety of natural and unnatural carbazoles may be prepared in a useful manner. Methoxycarbazole natural products glycoborine (**11**) and clausine V (**12**) are representative examples, with isolated yields of 77% and 75%, respectively. We note that the 2,7-dialkoxycarbazole motif as in **12** has found applications in electrochromic and optoelectronic materials, and the current catalytic protocol compares favorably with the commonly employed stoichiometric Cadogan methods used for preparation of this fragment. Complementarily, 2,7-substituted carbazoles bearing electron-withdrawing groups were also produced in good yield, albeit in somewhat lower overall yield (compare **13** and **2**).<sup>23</sup> Variation of the biaryl core provides access to related heterocarbazole derivatives, as in the functionalized  $\delta$ -carboline **14–17**. Both electron-withdrawing (**14–16**) and electron-donating substituents (**17**) are tolerated without incident. Fused polyheterocyclic compounds, including 7*H*-pyridocarbazole (**18**), are also capable of being prepared in good yield from the 5-aryl quinoline starting material.

**2.2.2 Synthesis of indoles and related heterocycles**—The catalytic protocol can be similarly applied to form indoles from various *o*-nitrostyrene compounds on a one-gram scale, although silica gel column chromatography proved to be more convenient for isolation

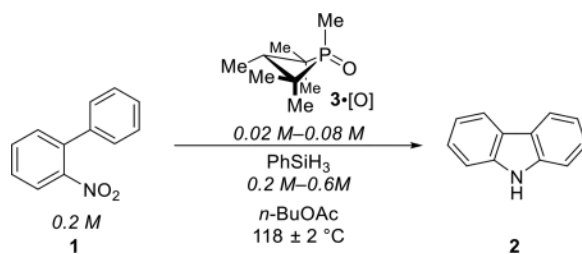
of these examples (Table 3). It was found that 2-substituted aryl indoles can be easily accessed under standard reaction conditions, providing 2-phenyl (**19**, **21**) and 2-mesityl (**20**) indole products with good yield. Nitrostyrene substrates bearing  $\alpha$ -aliphatic,  $\alpha,\beta$ -aliphatic, and  $\alpha,\beta$ -aromatic moieties were found to similarly cyclize to give the corresponding 3-substituted (**22**) and 2,3-disubstituted (**23**, **24**) indole products without incident. Additionally, 2-(2'-nitrophenyl)thiophene was cyclized to give 4*H*-thieno[3,2-*b*]indole (**25**) in good yield. A  $\gamma$ -pyrone bearing substrate was also readily cyclized to give pyrano[3,2-*b*]indole (**26**) in modest yield, which can be easily converted to the naturally occurring alkaloid koniamborine via *N*-methylation.<sup>24</sup> Biindole (**27**) could be prepared following mono-cyclization of (*E*)-3-(2-nitrostyryl)-1*H*-indole using our catalytic reaction conditions.

## 2.3 Mechanistic Investigations

**2.3.1 In situ spectral monitoring under catalytic conditions**—In situ spectral monitoring of the catalytic reaction was performed in order to gain insight into the reaction mechanism and to canvass for catalytic intermediates. <sup>1</sup>H NMR spectra (400 MHz, 100 °C) of a catalytic reaction (1 equiv of **1**, 20 mol% of **3**•[O], 2 equiv of phenylsilane, 1 M in toluene-*d*<sub>8</sub>) showed consumption of 2-nitrobiphenyl **1** over ca. 4 h with concomitant appearance of carbazole **2** as the major product. <sup>31</sup>P NMR spectra collected under identical conditions showed that phosphetane **3**•[O] ( $\delta$  53.5 ppm) is rapidly consumed ( $t_{1/2}$ ~5 min), giving rise to two new resonances at  $\delta$  32.5 and  $\delta$  19.0 ppm in a 5:1 ratio (Figure 2). Independent synthesis confirms that these signals correspond to the diastereomers of tricoordinate phosphetane **3** ( $\delta$  32.5 (major, *anti*);  $\delta$  19.0 ppm (minor, *syn*)). In accord with extensive literature precedent,<sup>25</sup> the lack of stereospecificity in the phosphetane *P*-oxide reduction event is taken to be indicative of the intermediacy of a pentacoordinate phosphorane with a sufficient lifetime during hydrosilane-mediated phosphine oxide reduction to permit pseudorotation leading to stereochemical scrambling.

As the catalytic conversion of **1** continues, the tricoordinate epimers of **3** remain the only observable phosphorus-containing compounds in solution. Evidently, tricoordinate **3** represents the catalytic resting state. When taken together, it can be inferred from the <sup>1</sup>H and <sup>31</sup>P NMR data that the turnover-limiting step in the catalytic formation of carbazole **2** involves an initial reaction of substrate **1** with tricoordinate phosphetane **3**, and that phosphine oxide reduction of **3**•[O] is more rapid than *O*-atom transfer to **3** from the 2-nitrobiphenyl substrate **1**.

**2.3.2 Catalytic reaction kinetics**—The kinetic progress of standard catalytic reaction (eq 1; conditions: 1 equiv of **1**, 20 mol% **3**•[O], 2 equiv of phenylsilane, 1 M in *n*-butyl acetate, 118  $\pm$  2 °C) was monitored quantitatively via ex situ HPLC analysis of reaction aliquots drawn at intervals over the course of 5 h.

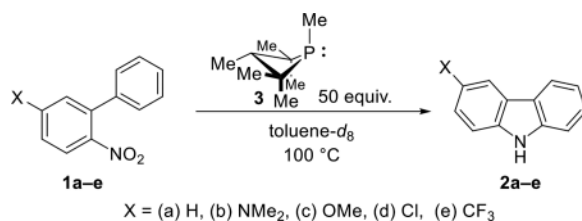


(1)

From the chromatograms (see Supporting Information), starting material **1** is converted to carbazole product **2** in >95 % efficiency. Plots depicting the depletion in concentration of starting material **1** as a function of time are fit by a model describing first order dependence in **1** (Figure 3A). The initial rates obtained via this method vary linearly with precatalyst **3•[O]** concentration in the range 0.02 M [b3•[O]] 0.08 M (Figure 3C), indicating that the reaction in eq 1 is pseudo-first order in precatalyst **3•[O]**. Rate constants obtained by the complementary monitoring of increasing product **2** concentration with time at varying precatalyst **3•[O]** concentrations (Figure 3B) agree within  $\pm 10\%$ . Initial reaction rates measured for this same catalytic reaction do not vary as a function of phenylsilane concentration in the range 0.2 M–0.6 M (Figure 3D), and therefore the reaction rate is zeroth order in phenylsilane within this concentration regime. Taken together, the empirical rate law for the catalytic Cadogan cyclization *o*-nitrobiphenyl may be described as in eq 2:

$$\nu = k_{\text{expt}} [\mathbf{1}]^1 [\mathbf{3} \bullet [\text{O}]]^1 [\text{PhSiH}_3]^0 \quad (2)$$

**2.3.3 Hammett linear free energy relationship**—In order to evaluate the electronic demand of the reaction, a panel of electronically varied 5-substituted 2-nitrobiphenyl compounds (**1a–e**) were treated under pseudo-first order conditions with an excess of phosphatane **3**, and the rates of conversion to the corresponding carbazoles (**2a–e**) were monitored over time relative to an internal standard (1,3,5-trimethoxybenzene) via  $^1\text{H}$  NMR spectroscopy (eq 3).

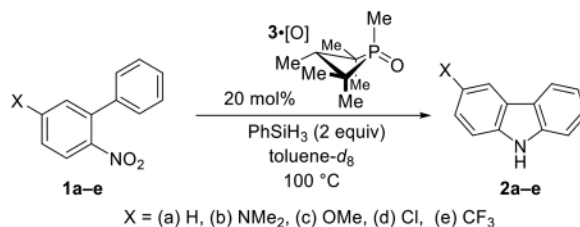


(3)

Qualitatively, a clear trend in relative rates for carbazole formation was observed, with substrates bearing electron-withdrawing 5-substituents proceeding to product more swiftly than those with electron-donating 5-substituents. A plot of  $\log(k_X/k_H)$  versus substituent

constant  $\sigma_p$  gives a good linear fit (Figure 4), from which a Hammett sensitivity constant  $\rho = +1.55$  may be derived. Evidently, the rate-determining transition structure for the transformations **1a–e** to **2a–e** is one in which partial negative charge accrues to the nitroarene moiety as might be expected for a reaction that reduces the oxidation state of the nitrogen center. These data are consistent with linear free energy relationships obtained by Sundberg<sup>26</sup> and Cadogan<sup>27</sup> with triethylphosphite and related P(III) reagents.

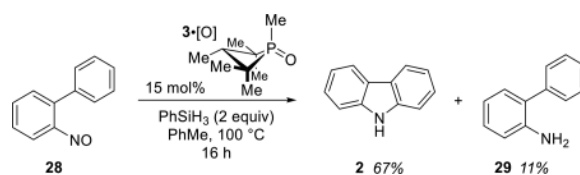
To compare this stoichiometric linear free energy relationship to one under catalytic conditions, the identical substrate set was transformed by reaction with 20 mol% **3**•[O], 2 equiv of phenylsilane, at 100 °C in toluene-*d*<sub>8</sub> (eq 4).



(4)

As in the stoichiometric studies, a positive Hammett sensitivity constant identical within experimental error ( $\rho = +1.55$ ) was obtained for the catalytic reaction (see Figure S1). This result adduces evidence that both the stoichiometric and catalytic reactions proceed in a mechanistically consistent manner in which the tricoordinate phosphetane **3** engages the nitroarene substrate in a rate-determining step involving net transfer of electron-density from the phosphorus compound to the nitro substrate.

**2.3.4 Studies on nitrosobiaryl substrates**—Despite the apparent absence of detectable intermediates during in situ spectroscopic monitoring, it seemed reasonable to consider the potential intermediacy of 2-nitrosobiphenyl (**28**). Previous studies on reductive nitroarene transformations have considered nitrosoarenes to be obligate intermediates, and Cadogan has specifically shown the stoichiometric conversion of 2-nitrosobiphenyl to carbazole with P(OEt)<sub>3</sub>.<sup>28</sup> A control experiment in which 2-nitrosobiphenyl (**28**) was subjected to catalytic conditions (eq 5) was found to produce 67% of carbazole **2** in addition to 11% of 2-aminobiphenyl (**29**). This result suggests that 2-nitrosobiphenyl is indeed a viable intermediate en route to carbazole under catalytic conditions, although alternative pathways compete at the relatively high concentrations of **28** in eq 5. The origin of the reduced product **29** remains a topic of investigation.



(5)



In an attempt to further investigate the reaction of 2-nitrosobiphenyl (**28**) with phosphetane **3**, low temperature VT-NMR studies were conducted. In a representative experiment (eq 6), a toluene-*d*<sub>8</sub> solution of **3** (0.13 M) was frozen in liquid nitrogen, and a cold (−78 °C) solution of 2-nitrosobiphenyl (**28**, 0.11 M, 1.3 equiv) was layered on top via syringe injection.



(6)

The resulting heterogeneous mixture was inserted into a −60 °C thermostatted NMR probe, where it underwent thawing and slow diffusional mixing over the course of ca. 80 min. <sup>31</sup>P NMR spectra (Figure 5) recorded subsequently at 10 min intervals showed the initial consumption of the starting tricoordinate phosphetane **3** (δ 24.2 *major*, 11.3 *minor* ppm)<sup>29</sup> and conversion to two new resonances with an upfield chemical shift (δ −24.4 *major*, −21.8 *minor* ppm). At subsequent time points, the resonances from these intermediates diminished, concomitant with growth of signals corresponding to **3**•[O] (δ 54.1 *major*, 61.8 *minor* ppm). Upon termination of the NMR experiment, an aliquot of the mixture was submitted to GCMS analysis, which showed the presence of phosphetane *P*-oxide **3**•[O] and carbazole **2** as the only observable products.

On the basis of the foregoing experiment, we postulate that the observed <sup>31</sup>P NMR resonance at δ −24.4 ppm corresponds to a metastable intermediate along the C–N bond forming carbazolation pathway, arising from reaction of phosphetane **3** and 2-nitrosobiphenyl (**28**). Furthermore, reaction between phosphetane **3** and isotopically labelled 2-(<sup>15</sup>N)nitrosobiphenyl shows that the resonance at δ −24.4 ppm exhibits <sup>31</sup>P–<sup>15</sup>N scalar coupling with *J* = 40.8 Hz (Figure 6A). The magnitude of this coupling constant falls within the expected range for direct one-bond <sup>1</sup>*J*<sub>P<sub>N</sub></sub> coupling,<sup>30</sup> and the upfield <sup>31</sup>P chemical shift is most consistent with a formulation as a pentacoordinate phosphorane species.<sup>17b,31</sup> A complementary doublet centered at δ 239 ppm (*J* = 40.6 Hz) is observed in the <sup>15</sup>N NMR spectrum. We therefore posit that P<sup>V</sup> oxazaphosphirane structures **30**, as depicted in eq 6, give rise to the observed intermediate <sup>31</sup>P NMR resonances. Compounds **30** would be formed from **3** as two magnetically inequivalent stereoisomers (*anti*-**30** and *syn*-**30**) that could account for the observed signals in the heteronuclear NMR spectra.

The geometries of DFT models for diastereomers *anti*-**30** and *syn*-**30** were optimized at the M06-2X/6–311++G(d,p) level of theory (Figure 6C), and the magnetic shielding tensors for these species were computed by the gauge-independent atomic orbital (GIAO) routine at the PBE1PBE/6–311G(2d,2p) level. The predicted isotropic chemical shifts for *anti*-**30** and *syn*-**30** (δ −26.8 and −28.8 ppm, respectively) are in good agreement with the observed signals in the low temperature <sup>31</sup>P NMR spectra depicted in Figure 6. As a further measure of confidence in the predicted NMR shift for **30**, we similarly computed GIAO <sup>31</sup>P NMR chemical shifts for the epimers of **3** and **3**•[O], whose structures and spectra are

independently known from experiment (Table 4). The linear correlation between observed and calculated  $^{31}\text{P}$  NMR chemical shifts (Figure S7) provides an internal validation that the GIAO routine renders a quality description (average error of  $\delta \pm 5$  ppm) of the isotropic chemical shift in this series of experimentally relevant phosphetane compounds. The general suitability of GIAO-DFT methods for the prediction of  $^{31}\text{P}$  NMR chemical shifts has recently been analyzed by Latypov and coworkers.<sup>32</sup>

## 2.4 Computational Modeling of the Reaction Sequence

### 2.4.1 DFT studies of the first deoxygenation event – mechanism of nitroarene deoxygenation

—In an effort to gain a more atomistic understanding of the mechanism of catalytic Cadogan cyclization, potential energy surface modeling of the two sequential deoxygenations of 2-nitrobiphenyl (**1**) by phosphetane **3** were conducted at the M06-2X/6-311++G(d,p) level of theory with a polarizable continuum model (PCM) for solvation in *n*-butyl acetate ( $\epsilon = 4.9941$ ). In accord with our previous calculations on a related system,<sup>18</sup> computational models indicate a stepwise pathway for the initial deoxygenation of **1** by phosphetane **3** proceeding by (3+1) cheletropic addition (**TS1**,  $G_{\text{rel}}^{\ddagger} = +30.0$  kcal/mol) to form pentacoordinate spiro-bicyclic dioxazaphosphetane species **INT1** (Figures 7 and 8). Both the P–O (2.39 Å and 2.21 Å) and N–O (1.28 Å and 1.27 Å) bond distances in **TS1** are indicative of a concerted mechanism in which the phosphorous concurrently attacks the two oxygen atoms of the nitro group. The heteroatomic ring system of **INT1** displays a nearly planar four-membered ring ( $D_{\text{PONO}} = 6.7^\circ$ ) that includes a square pyramidal phosphorus and a pyramidal nitrogen.

Subsequent evolution of dioxazaphosphetane **INT1** produces phosphine oxide **3•[O]** and 2-nitrosobiphenyl (**28**) by a retro-(2+2) fragmentation. This step is computed to be significant downhill energetically ( $G_{\text{rel}} = -35.8$  kcal/mol), with comparatively low kinetic barrier via **TS2** ( $G_{\text{rel}}^{\ddagger} = +11.8$  kcal/mol). The low activation energy of the cycloreversion is consistent with ring strain relief and the advanced formation of phosphetane *P*-oxide **3•[O]**.

The calculated (3+1) pathway is adequate to account for the observed linear free energy correlation (see Sect. 2.3.3). DFT energy barriers computed for the (3+1) cheletropic addition of 5-substituted 2-nitrobiphenyls with **3** (Table 5) reproduce with good quantitative agreement the trend observed experimentally in Figure 4; namely, that electron-withdrawing substituents accelerate the rate of formal (3+1) cheletropic addition.

### 2.4.2 DFT studies of the second deoxygenation event – mechanism of nitrosoarene deoxygenation and C–N bond formation

—Modeling the deoxygenation of 2-nitrosobiphenyl **28** by phosphetane **3** revealed the favorable formation of oxazaphosphirane intermediates **30** ( $G_{\text{rel}} = -3.7$  kcal/mol for the most stable *anti*-**30** diastereomer, shown in Figure 9). The transition structure found for the (2+1) addition, **TS3** ( $G_{\text{rel}}^{\ddagger} = +24.8$  kcal/mol), is largely asynchronous and displays a bonding interaction between the lone pair of the phosphorus and the  $\pi^*(\text{N}=\text{O})$  orbital of the nitrosoarene (Figure 10, P–O = 2.01 Å).<sup>33</sup>

Efforts to locate transition structures associated with the collapse of oxazaphosphirane *anti*-**30** led to **TS4a** and **TS4b**, which describe two extremes in the bond forming sequence

toward the generation of carbazole (**2**) (Figure 10). Whereas **TS4a** represents the dissociative pathway in which phosphetane *P*-oxide **3•[O]** departs before the C–N bond is formed to generate biphenylnitrene **31**, **TS4b** corresponds to the associative pathway where C–N bond formation is fairly advanced before the departure of **3•[O]**. Estimation of the activation energies of **TS4a** and **TS4b** using the Yamaguchi spin projection method to account for spin contamination suggests that the dissociative pathway denoted by **TS4a** ( $G_{\text{rel}}^{\ddagger} = +11.9$  kcal/mol) is strongly favored compared to the associative pathway via **TS4b** ( $G_{\text{rel}}^{\ddagger} = +43.1$  kcal/mol). The incipient formation of the C–N bond in **TS4b** affords a highly ordered transition structure that, relative to intermediate *anti*-**30**, displays significant elongation of the P–N bond distance.<sup>34</sup> Taking into account that the combined dissociation products (singlet biphenylnitrene **31** and **3•[O]**) are computed to be  $G_{\text{rel}} = +2.2$  kcal/mol above the reactants and that the calculated activation energy reported for its cyclization via **TS5** is  $G_{\text{rel}}^{\ddagger} = +6.9$  kcal/mol,<sup>35,36</sup> the computations are consistent with the experimental detection of intermediates **30** and the non-limiting barrier measured for their collapse to afford carbazole (**2**).

### 3. discussion

The synthetic method described above represents a robust and process scalable organocatalytic approach to the synthesis of carbazoles and indoles from appropriately decorated nitroarene substrates. In view of the operational simplicity and comparatively mild conditions of the catalytic reaction protocol, it might be expected that this approach could supplant traditional stoichiometric Cadogan cyclization in circumstances where it is currently employed.

With respect to the function of the phosphorus-based catalyst, the results of both synthetic and spectral investigations are consistent with the requirement for interconversion of **3** and **3•[O]** during the course of the catalysis via  $\text{P}^{\text{III}}/\text{P}^{\text{V}}=\text{O}$  redox cycling. It has long been held that the central impediment to catalysis in the  $\text{P}^{\text{III}}/\text{P}^{\text{V}}=\text{O}$  couple stems from the kinetic and thermodynamic inertness of phosphine oxide P=O bond. Despite these notions, we find in the case of this catalytic Cadogan system that in situ reduction of the phosphine oxide is not turnover limiting. Instead, the small ring phosphacycle in **3•[O]** exhibits a high rate of P=O deoxygenation by hydrosilane reductant to the tricoordinate phosphetane **3**, which represents the resting state of the catalytic cycle. The rapid rate with which **3•[O]** is deoxygenated falls in line with precedent regarding the swift deoxygenation of cyclic phosphine oxides,<sup>20b,20d,37</sup> and builds on fundamental notions of enhanced electrophilic reactivity of constrained phosphacycles.<sup>38</sup>

The phosphorus-based catalyst operates on the nitro substrate to effect double deoxygenation in a stepwise fashion. The first deoxygenation step is gated kinetically by a pericyclic (3+1) cheletropic addition, which can be understood with the nitro substrate expressing orbital character as a  $4\pi_s$  component<sup>39</sup> and the phosphetane as a  $2\omega_s$  component.<sup>17b,18</sup> Both the experimental and computed Hammett correlations are in good agreement, providing an affirmative benchmark for this DFT pathway. The proposed (3+1)-pathway has not typically been invoked in Cadogan chemistry (where proposals of acyclic zwitterionic intermediates have prevailed<sup>9,13b</sup>); the data presented here provide evidence, albeit indirect,

for the intervention of such an ephemeral four-membered ring intermediate in phosphine/nitroarene reactions. The second deoxygenation step again involves an all-heteroatom cyclic intermediate, but spectroscopic identification is permitted in this case. Heteronuclear NMR spectroscopy, bolstered by GIAO-DFT modeling, provide evidence for the formation of an oxazaphosphirane upon low temperature mixing of phosphetane **3** and 2-nitrosobiphenyl. Both Cadogan<sup>40</sup> and Sundberg<sup>26</sup> have speculated on the involvement of an oxazaphosphirane species in the reaction pathway leading to product, but such a species has not been directly observed. We believe that our spectra represent the first characterization of the unusual all-heteroatom (ONP) small-ring system. It seems likely that thermal decomposition of this oxazaphosphirane intermediate above ca. -50 °C leads to dissociation of phosphetane **3**•[O] with conversion of biarylnitrene residue to carbazole. Via this pathway, the system here converges with the extensive body of experimental and theoretical literature concerning the electronic configuration and ring-closing reactivity of 2-biphenylnitrene.<sup>35</sup>

The sequence of elementary steps proposed for nitroarene double deoxygenation is usefully contextualized by isolobal analogy to the reactions of tricoordinate phosphorus compounds with ozone and singlet oxygen (Figure 11). It is well-known that phosphines and phosphites undergo formal (3+1) addition of O<sub>3</sub> to form cyclic ozonides (R<sub>3</sub>P•O<sub>3</sub>) with pentacoordinated phosphorus centers contained within a four-membered trioxaphosphetane (i.e. O<sub>3</sub>P) ring system,<sup>41</sup> which in view of the significant thermodynamic driving force for adduct formation occur with near diffusion-controlled rates. Subsequent thermal decomposition of the phosphine(-ite) ozonides **I** eliminates one equivalent of phosphine oxide and gives <sup>1</sup>O<sub>2</sub>.<sup>41,42</sup> In the case of the proposed (3+1) addition of nitroarenes to phosphines, the thermodynamic driving force for cheletropic addition is greatly diminished as compared to the O<sub>3</sub> analogue; the kinetic barrier to adduct formation is consequently increased to the extent that it becomes kinetically limiting to catalysis. The azadioxophosphetane adducts **III** are therefore not observable and instead proceed to fragment in retro-(2+2) fashion with elimination of an equivalent of phosphine oxide and formation of a nitrosoarene byproduct.

Continuing the isolobal analogy, singlet oxygen has been shown to react with tricoordinate phosphorus to give adducts that have been spectroscopically characterized by Selke at low temperature as pentacoordinate dioxaphosphiranes (R<sub>3</sub>P•O<sub>2</sub>, **II**).<sup>43</sup> These R<sub>3</sub>PO<sub>2</sub> compounds behave as electrophilic oxene donors with loss of R<sub>3</sub>PO, in much the same way that the proposed oxazaphosphirane **IV** (*viz.* **30**) exhibits nitrene-like ability to aminate proximal C<sub>sp2</sub>-H bonds. The extent to which the deoxygenation of nitro compounds by small-ring phosphacycles via the proposed oxazaphosphirane serves as a general organophosphorus-catalyzed entry into nitrene- or nitrenoid-reactivity is a matter of ongoing study.

## 4. Conclusion

We have demonstrated a catalytic Cadogan synthesis of useful carbazole and indole products with a small-ring phosphacycle catalyst and hydrosilane terminal reductant. Experimental and computational modeling results implicate the operation of a P<sup>III</sup>/P<sup>V</sup>=O redox cycle in which phosphine **3** is the resting state and initial deoxygenation of the nitro substrate

represents the turnover-limiting step.  $^{31}\text{P}$  NMR spectral monitoring and modeling of the second deoxygenation event imply the intervention of a spirocyclic pentacoordinate phosphorus intermediate exhibiting an unprecedented oxazaphosphirane ring system, the decomposition of which leads to carbazole product with loss of phosphetane *P*-oxide through a nitrenoid pathway. Additional studies on the structure and reactivity of pentacoordinate oxazaphosphirane species of this type are warranted. Finally, the mechanistic hypotheses advanced in this study provide a framework for future biphilic organophosphorus catalyst design and for reaction development within this  $\text{P}^{\text{III}}/\text{P}^{\text{V}}=\text{O}$  manifold, both of which constitute active ongoing research aims in our laboratories.

## 5. EXPERIMENTAL SECTION

A full description of the general experimental methods can be found in the Supporting Information.

### 5.1 Representative Synthetic Procedure for Carbazoles

To a 40 mL screw-cap vial fitted with a stir bar was added 1 gram of *o*-nitrobiphenyl substrate, 20 mol% of phosphetane oxide precatalyst **3**•[O], *n*-butyl acetate (1 M), and phenylsilane (2 equiv). A cap was screwed on and the reaction was heated at 120 °C with stirring until TLC indicated the completion of reaction. Following cyclization, the homogeneous reaction mixture was cooled to room temperature, during which time a precipitate was formed. The solids were collected on a glass frit and washed with one portion of  $\text{CH}_2\text{Cl}_2$  to yield the carbazole products with >98% purity by HPLC analysis.

### 5.2 Representative Synthetic Procedure for Indoles

To a flame-dried 25 mL round-bottom flask fitted with a stir bar was added 1 gram of *o*-nitrostyrene substrate, 20 mol% of phosphetane oxide precatalyst **3**•[O], and a septum. Following evacuation and the introduction of nitrogen on a Schlenk line, dry *n*-butyl acetate (1 M) was added via syringe from a SureSeal bottle. Phenylsilane (2 equiv) was added lastly and heating/stirring (120 °C, ~500 rpm) was continued under positive nitrogen until TLC indicated the completion of the reaction. Following completion, the sample was allowed to cool and 10 mL of 3–6 M HCl was added. The organic layer was separated and the aqueous layer was extracted with ethyl acetate (2×25 mL). The combined organic layer was then dried over anhydrous sodium sulfate and concentrated in vacuo. Column chromatography on silica subsequently afforded the desired indole products.

### 5.3 Kinetics Experiments

For a kinetic run corresponding to a single rate constant, a solution of 2-nitrobiphenyl (**1**) and phosphetane *P*-oxide **3**•[O] in *n*-butyl acetate was prepared under nitrogen in an oven-dried, three-neck round-bottom flask fitted with a silicon-tipped IR probe and a magnetic stir bar. The solution temperature was stabilized at  $108 \pm 2$  °C and the reaction was initiated by adding phenylsilane. Reaction monitoring started 15 min after the addition of phenylsilane to ensure full reduction of **3**•[O] as determined by disappearance of the *P*-oxide IR absorbance at  $1195\text{ cm}^{-1}$ . Sample aliquots ( $20\text{ }\mu\text{L} \pm 10\%$ ) were periodically taken using a calibrated automated sampler,<sup>44</sup> diluted at room temperature into *n*-butyl acetate (80×) and

analyzed using an HPLC system equipped with a C18 column (4.6 × 50 mm) and a SPD-20A/20AV UV–vis detector. Good pseudo-first-order plots were obtained by monitoring the growth of carbazole (**2**) relative to a standard calibration curve and the initial rates ( $[1]/t$ ) were calculated by multiplying the pseudo-first-order reaction rate constants (exponential slopes) by the corresponding concentrations of 2-nitrophenyl (**1**). Rates were shown to be reproducible within experimental error ( $\pm 10\%$ ).

#### 5.4 Computational Methods

Geometries were optimized in Gaussian 09<sup>45</sup> using the M06-2X<sup>46</sup> density functional with the 6-311++G(d,p) basis set. The calculated energies ( $G$ , 298.15 K, 1.0 atm) result from the sum of electronic and thermal free energies as obtained from the frequency analysis at the same level of theory. Frequency calculations for all stationary points were carried out to describe them either as minima ( $i = 0$ ) or as first-order transition states ( $i = 1$ ). For all transition structures, visualization of the imaginary frequencies corresponded to the expected normal mode for the elementary step under investigation. Intrinsic reaction coordinate calculations (IRC) were performed from the transition states in forward and reverse directions to confirm the lowest energy reaction pathways that connect the corresponding minima. See Supporting Information for further details.

#### Supplementary Material

Refer to Web version on PubMed Central for supplementary material.

#### Acknowledgments

Financial support was provided by NIH NIGMS (GM114547), MIT, and Bristol-Myers Squibb. We thank the Buchwald laboratory (MIT) for access to equipment and chemicals.

#### References

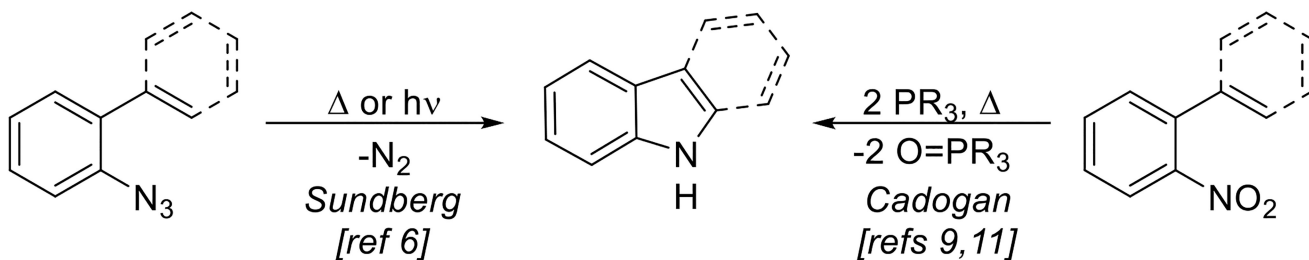
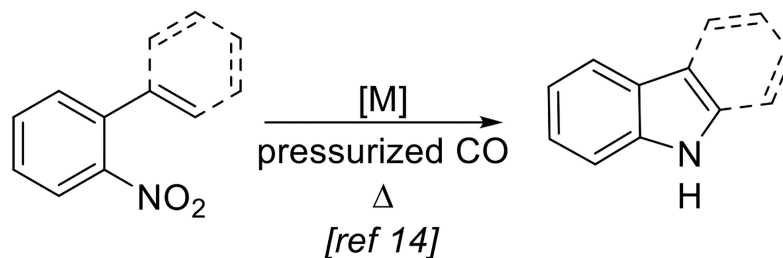
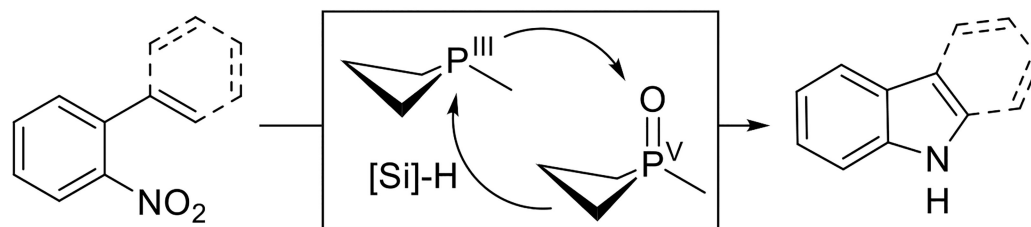
1. (a) Schmidt AW, Reddy KR, Knölker H-J. *Chem. Rev.* 2012; 112:3193. [PubMed: 22480243] (b) Kaushik NK, Kaushik N, Attri P, Kumar N, Kim CH, Verma AK, Choi EH. *Molecules.* 2013; 18:6620. [PubMed: 23743888]
2. (a) Justin Thomas KR, Lin JT, Tao Y-T, Ko C-W. *J. Am. Chem. Soc.* 2001; 123:9404. [PubMed: 11562223] (b) Blouin N, Michaud A, Gendron D, Wakim S, Blair E, Neagu-Plesu R, Belletête M, Durocher G, Tao Y, Leclerc M. *J. Am. Chem. Soc.* 2008; 130:732. [PubMed: 18095689] (c) Gendron D, Leclerc M. *Energy Environ. Sci.* 2011; 4:1225. (d) Sathiyam G, Sivakumar EKT, Ganesamoorthy R, Thangamuthu R, Sakthivel P. *Tetrahedron Lett.* 2016; 57:243. (e) Rajamalli P, Senthilkumar N, Huang P-Y, Ren-Wu C-C, Lin H-W, Cheng C-H. *J. Am. Chem. Soc.* 2017; 139:10948. [PubMed: 28745874]
3. Roy J, Jana AK, Mal D. *Tetrahedron.* 2012; 68:6099.
4. (a) Taber DF, Tirunahari PK. *Tetrahedron.* 2011; 67:7195. [PubMed: 25484459] (b) Humphrey GR, Kuethe JT. *Chem. Rev.* 2006; 106:2875. [PubMed: 16836303]
5. (a) Tsang WCP, Zheng N, Buchwald SL. *J. Am. Chem. Soc.* 2005; 127:14560. [PubMed: 16231894] (b) Jordan-Hore JA, Johansson CCC, Gulias M, Beck EM, Gaunt MJ. *J. Am. Chem. Soc.* 2008; 130:16184. [PubMed: 18998652] (c) Tsang WCP, Munday RH, Brasche G, Zheng N, Buchwald SL. *J. Org. Chem.* 2008; 73:7603. [PubMed: 18761437] (d) Cho SH, Yoon J, Chang S. *J. Am. Chem. Soc.* 2011; 133:5996. [PubMed: 21446710] (e) Takamatsu K, Hirano K, Satoh T, Miura M. *Org. Lett.* 2014; 16:2892. [PubMed: 24813821] (f) Suzuki C, Hirano K, Satoh T, Miura M. *Org. Lett.* 2015; 17:1597. [PubMed: 25760543]

6. (a) Smith PAS, Brown BB. *J. Am. Chem. Soc.* 1951; 73:2435.(b) Sundberg RJ, Lin L-S, Blackburn DE. *J. Heterocyclic Chem.* 1969; 6:441.(c) Sundberg RJ, Russell HF, Ligon WV, Lin L-S. *J. Org. Chem.* 1972; 37:719.(d) Lindley JM, McRobbie IM, Meth-Cohn O, Suschitzky H. *J. Chem. Soc. Perkin Trans. 1.* 1977; 0:2194.
7. (a) Shen M, Leslie BE, Driver TG. *Angew. Chem. Int. Ed.* 2008; 47:5056.(b) Stokes BJ, Jovanovi B, Dong H, Richert KJ, Riell RD, Driver TG. *J. Org. Chem.* 2009; 74:3225. [PubMed: 19296584] (c) Sun K, Liu S, Bec PM, Driver TG. *Angew. Chem. Int. Ed.* 2011; 50:1702.(d) Pumphrey AL, Dong H, Driver TG. *Angew. Chem. Int. Ed.* 2012; 51:5920.
8. (a) Archibald, T. *Managing Hazardous Reactions and Compounds in Process Chemistry*; ACS Symposium Series. Vol. 1181. American Chemical Society; Washington, DC: 2014. p. 87-109.(b) González-Bobes F, Kopp N, Li L, Deerberg J, Sharma P, Leung S, Davies M, Bush J, Hamm J, Hrytsak M. *Org. Process Res. Dev.* 2012; 16:2051.
9. (a) Cadogan JIG, Cameron-Wood M, Mackie RK, Searle RJG. *J. Chem. Soc.* 1965:4831.(b) Cadogan JIG. *Q. Rev. Chem. Soc.* 1968; 22:222.
10. (a) Ono, N. *The Nitro Group in Organic Synthesis*. Wiley; New York, NY: 2001. (b) Gui J, Pan C-M, Jin Y, Qin T, Lo JC, Lee BJ, Spengel SH, Mertzman ME, Pitts WJ, Cruz TEL, Schmidt MA, Darvatkar N, Natarajan SR, Baran PS. *Science.* 2015; 348:886. [PubMed: 25999503] (c) Bartoli G, Dalpozzo R, Nardi M. *Chem. Soc. Rev.* 2014; 43:4728. [PubMed: 24718836]
11. Genung NE, Wei L, Aspnes GE. *Org. Lett.* 2014; 16:3114. [PubMed: 24848311]
12. (a) Dohle W, Staubitz A, Knochel P. *Chem. Eur. J.* 2003; 9:5323. [PubMed: 14613142] (b) Wróbel Z, Wojciechowski K. *Synlett.* 2011; 2011:2567.(c) Gao H, Xu Q-L, Yousufuddin M, Ess DH, Kürti L. *Angew. Chem. Int. Ed.* 2014; 53:2701.(d) Tong S, Xu Z, Mamboury M, Wang Q, Zhu J. *Angew. Chem. Int. Ed.* 2015; 54:11809.(e) Yang K, Zhou F, Kuang Z, Gao G, Driver TG, Song Q. *Org. Lett.* 2016; 18:4088. [PubMed: 27499149]
13. (a) Appukkuttan P, Eycken EVder, Dehaen W. *Synlett.* 2005; 2005:127.(b) Freeman AW, Urvoy M, Criswell ME. *J. Org. Chem.* 2005; 70:5014. [PubMed: 15960500] (c) Creencia EC, Kosaka M, Muramatsu T, Kobayashi M, Iizuka T, Horaguchi T. *J. Heterocyclic Chem.* 2009; 46:1309.(d) Peng H, Chen X, Chen Y, He Q, Xie Y, Yang C. *Tetrahedron.* 2011; 67:5725.
14. (a) Akazome M, Kondo T, Watanabe Y. *J. Org. Chem.* 1994; 59:3375.(b) Söderberg BC, Shriver JA. *J. Org. Chem.* 1997; 62:5838.(c) Smitrovich JH, Davies IW. *Org. Lett.* 2004; 6:533. [PubMed: 14961616] (d) Davies IW, Smitrovich JH, Sidler R, Qu C, Gresham V, Bazaraal C. *Tetrahedron.* 2005; 61:6425.(e) Hsieh THH, Dong VM. *Tetrahedron.* 2009; 65:3062.
15. Shevlin M, Guan X, Driver TG. *ACS Catal.* 2017; 7:5518.
16. Kirby, AJ., Warren, SG. *The Organic Chemistry of Phosphorus*. Elsevier; Amsterdam: 1967. p. 20
17. (a) Dunn NL, Ha M, Radosevich AT. *J. Am. Chem. Soc.* 2012; 134:11330. [PubMed: 22746974] (b) Reichl KD, Dunn NL, Fastuca NJ, Radosevich AT. *J. Am. Chem. Soc.* 2015; 137:5292. [PubMed: 25874950] (c) Zhao W, Yan PK, Radosevich AT. *J. Am. Chem. Soc.* 2015; 137:616. [PubMed: 25564133]
18. Nykaza TV, Harrison TS, Ghosh A, Putnik RA, Radosevich AT. *J. Am. Chem. Soc.* 2017; 139:6839. [PubMed: 28489354]
19. (a) Marsden SP, McGonagle AE, McKeever-Abbas B. *Org. Lett.* 2008; 10:2589. [PubMed: 18489173] (b) Denton RM, An J, Adeniran B. *Chem. Commun.* 2010; 46:3025.(c) Denton RM, Tang X, Przeslak A. *Org. Lett.* 2010; 12:4678. [PubMed: 20845932] (d) Denton RM, An J, Adeniran B, Blake AJ, Lewis W, Poulton AM. *J. Org. Chem.* 2011; 76:6749. [PubMed: 21744876] (e) Denton RM, An J, Lindovska P, Lewis W. *Tetrahedron.* 2012; 68:2899.(f) An J, Tang X, Moore J, Lewis W, Denton RM. *Tetrahedron.* 2013; 69:8769.(g) Marsden, SP. *Sustainable Catalysis*. Dunn, PJ.Hii, KK(Mimi)Krische, MJ., Williams, MT., editors. John Wiley & Sons Inc.; Hoboken, NJ: 2013. p. 339-361.(h) Yu T-Y, Wang Y, Xu P-F. *Chem. Eur. J.* 2014; 20:98. [PubMed: 24285309] (i) Wang L, Qin R-Q, Yan H-Y, Ding M-W. *Synthesis.* 2015; 47:3522.(j) Yan Y-M, Rao Y, Ding M-W. *J. Org. Chem.* 2016; 81:1263. [PubMed: 26759921]
20. (a) O'Brien CJ, Tellez JL, Nixon ZS, Kang LJ, Carter AL, Kunkel SR, Przeworski KC, Chass GA. *Angew. Chem. Int. Ed.* 2009; 48:6836.(b) van Kalkeren HA, Leenders SHAM, Hommersom CRA, Rutjes FPJT, van Delft FL. *Chem. Eur. J.* 2011; 17:11290. [PubMed: 21882274] (c) O'Brien CJ, Lavigne F, Coyle EE, Holohan AJ, Doonan BJ. *Chem. Eur. J.* 2013; 19:5854. [PubMed: 23526683] (d) O'Brien CJ, Nixon ZS, Holohan AJ, Kunkel SR, Tellez JL, Doonan BJ, Coyle EE,

- Lavigne F, Kang LJ, Przeworski KC. Chem. Eur. J. 2013; 19:15281. [PubMed: 24115040] (e) van Kalkeren HA, te Grotenhuis C, Haasjes FS, Hommersom C(Rianne)A, Rutjes FPJT, van Delft FL. Eur. J. Org. Chem. 2013; 2013:7059.(f) Tsai Y-L, Lin W. Asian J. Org. Chem. 2015; 4:1040.(g) Lee C-J, Chang T-H, Yu J-K, Madhusudhan Reddy G, Hsiao M-Y, Lin W. Org. Lett. 2016; 18:3758. [PubMed: 27434727] (h) Saleh N, Voituriez A. J. Org. Chem. 2016; 81:4371. [PubMed: 27080174] (i) Schirmer M-L, Adomeit S, Spannenberg A, Werner T. Chem. Eur. J. 2016; 22:2458. [PubMed: 26762186] (j) Voituriez A, Saleh N. Tetrahedron Lett. 2016; 57:4443.
21. van Kalkeren HA, Blom AL, Rutjes FPJT, Huijbregts MAJ. Green Chem. 2013; 15:1255.
  22. Henderson RK, Jiménez-González C, Constable DJC, Alston SR, Inglis GGA, Fisher G, Sherwood J, Binks SP, Curzons AD. Green Chem. 2011; 13:854.
  23. The lower observed yields with some substrates bearing electron-withdrawing substituents correlate with an increase in undesired noncyclative reduction of the nitro group to the corresponding aniline. The identity of the hydrosilane reductant has some role in mitigating this pathway (cf. **13**), although the origin of this minor competing reduction remains under investigation.
  24. (a) Grougnet R, Magiatis P, Fokialakis N, Mitaku S, Skaltsounis A-L, Tillequin F, Sévenet T, Litaudon M. J. Nat. Prod. 2005; 68:1083. [PubMed: 16038554] (b) Clawson RW, Söderberg BCG. Tetrahedron Lett. 2007; 48:6019.
  25. (a) Mislow K. Acc. Chem. Res. 1970; 3:321.(b) Marinetti A, Carmichael D. Chem. Rev. 2002; 102:201. [PubMed: 11782133]
  26. Sundberg RJ, Lang C-C. J. Org. Chem. 1971; 36:300.
  27. Armour MA, Cadogan JIG, Grace DSB. J. Chem. Soc. Perkin Trans 2. 1975; 11:1185.
  28. Bunyan PJ, Cadogan JIG. J. Chem. Soc. 1963; 0:42.
  29. The  $^{31}\text{P}$  NMR chemical shifts of **3** and **3** $\cdot$ [O] exhibit temperature dependent behavior. See Supporting Information for plots of  $^{31}\text{P}$  NMR chemical shift temperature dependence for *syn*-**3** and *anti*-**3**. The temperature dependence of  $^{31}\text{P}$  NMR chemical shifts has been noted previously, see: Gordon MD, Quin LD. J. Magn. Reson. 1976; 22:149.
  30. (a) Gombler W, Kinan RW, Stec WJ. Z. Naturforsch. B. 1983; 38:815.(b) Viljanen T, Klika KD, Fülöp F, Pihlaja K. J. Chem. Soc. Perkin Trans. 2. 1998; 0:1479.
  31. Kojima S, Sugino M, Matsukawa S, Nakamoto M, Akiba K. J. Am. Chem. Soc. 2002; 124:7674. [PubMed: 12083918]
  32. Latypov SK, Polyancev FM, Yakhvarov DG, Sinyahsin OG. Phys. Chem. Chem. Phys. 2015; 17:6976. [PubMed: 25683906]
  33. Khursan VS, Shamukaev VA, Chainikova EM, Khursan SL, Safiullin RL. Russ. Chem. Bull. 2013; 62:2477.
  34. **TS4b** displays an N–O–P connectivity considered for the mechanism of oxygen transfer from nitrones to phosphines: Kurtzweil ML, Beak P. J. Am. Chem. Soc. 1996; 118:3426.
  35. For related DFT calculations of nitrene insertions, see: Tsao M-L, Gritsan N, James TR, Platz MS, Hrovat DA, Borden WT. J. Am. Chem. Soc. 2003; 125:9343. and references therein. [PubMed: 12889963]
  36. Calculation of the transition structure for the direct cyclization of 2-nitrosobiphenyl (**TS6** in Supporting Information) affords a high activation barrier,  $G_{\text{rel}}^{\ddagger} = +32.2$  kcal/mol, inconsistent with the mechanistic studies presented herein and indicative of a large preference for the nitrenoid pathway shown in Figure 10. For a discussion on the cyclization of nitrosoarenes, see: Davies IW, Guner VA, Houk KN. Org. Lett. 2004; 5:743.
  37. (a) Marsi KL. J. Am. Chem. Soc. 1969; 91:4724.(b) Marsi KL. J. Org. Chem. 1974; 39:265.(c) Keglevich G, Fekete M, Chuluunbaatar T, Dobó A, Harmat V, Tóke L. J. Chem. Soc. Perkin Trans. 2000; 1:4451.
  38. (a) Westheimer FH. Acc. Chem. Res. 1968; 1:70.(b) Hudson RF, Brown C. Acc. Chem. Res. 1972; 5:204.
  39. (a) Leitich J. Angew. Chem. Int. Ed. 1976; 15:372–373.(b) Balczewski P, Beddoes R, Joule JA. J. Chem. Soc. Chem. Commun. 1991:559.(c) Rudchenko VF. Chem. Rev. 1993; 93:725.
  40. Cadogan JIG, Todd MJ. J. Chem. Soc. C. 1969; 0:2808.



41. Murray, RW. Singlet Oxygen. Wasserman, HH., Murray, RW., editors. Academic Press; New York: 1979. p. 93-110.
42. Related retro-(2+2) fragmentations of this type are of course well-known in phosphorus ylide olefination pathways.
43. Ho DG, Gao R, Celaje J, Chung H-Y, Selke M. *Science*. 2003; 302:259. [PubMed: 14551430]
44. Accurate reaction sampling and dilution was performed using a probe-based Mettler-Toledo EasySampler 1210 system, see: Kerstin Z, Grosser S, Welch CJ. *Tetrahedron*. 2017; 73:5048.
45. Frisch, MJ., et al. Gaussian 09, revision B.01. Gaussian, Inc.; Wallingford, CT: 2009.
46. (a) Zhao Y, Truhlar DG. *Theor. Chem. Acc.* 2008; 120:215.(b) Zhao Y, Truhlar DG. *Acc. Chem. Res.* 2008; 41:157. [PubMed: 18186612]

**(A) Stoichiometric carbazole- and indole-forming C-H aminations****(B) Transition metal catalyzed azacyclization of nitroarenes****(C) This work: P<sup>III</sup>/P<sup>V</sup>=O catalyzed Cadogan cyclization**

**Figure 1.** Intramolecular C<sub>sp2</sub>-H amination reactions. (A) Classical Sundberg and Cadogan reactions. (B) Transition metal catalyzed carbazole-/indole-formation. (C) Catalytic Cadogan cyclization operating through a P<sup>III</sup>/P<sup>V</sup>=O redox cycle.

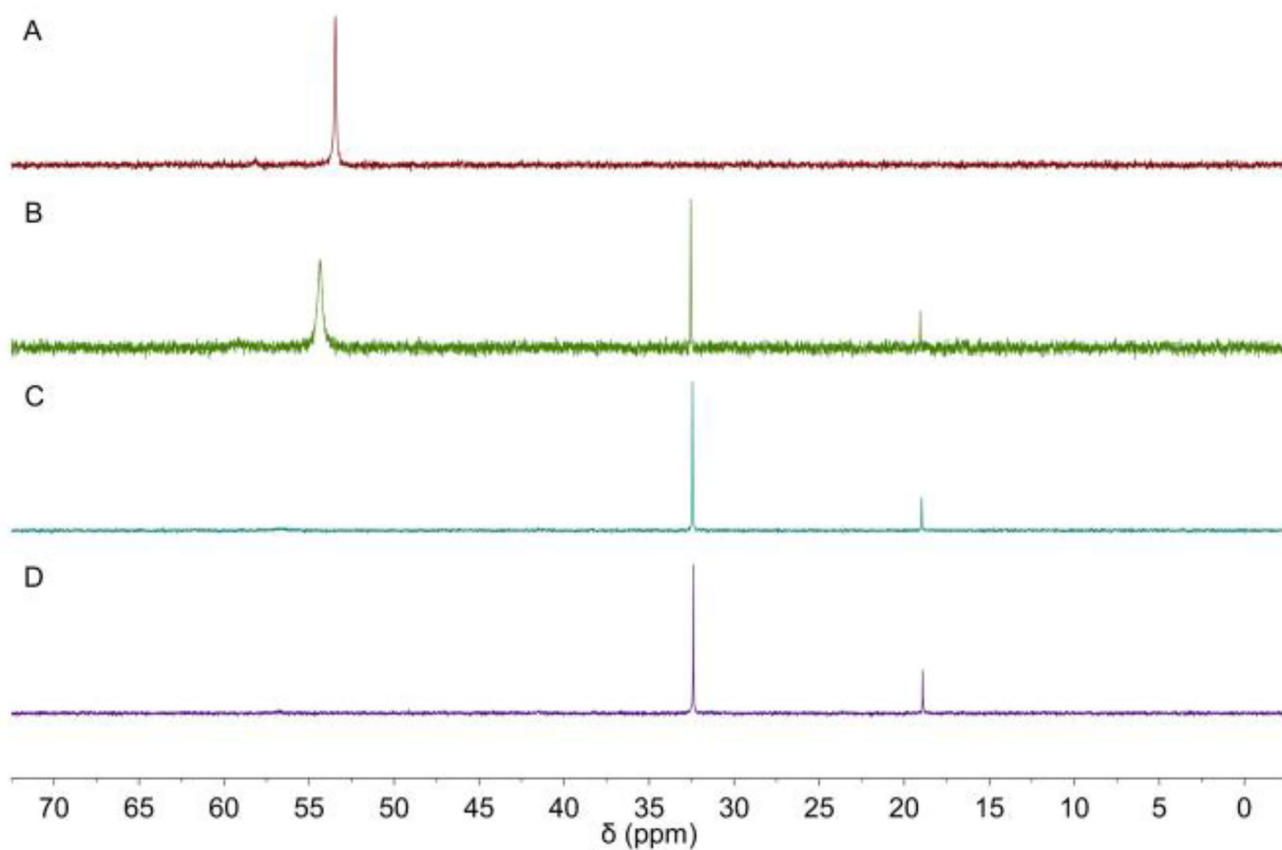


**Figure 2.** Time-stacked in situ  $^{31}\text{P}$  NMR spectra during catalysis ( $T = 100\text{ }^\circ\text{C}$ , toluene- $d_8$ ). (A)  $t = 0$  min; (B)  $t = 5$  min; (C)  $t = 30$  min; (D)  $t = 60$  min. Chemical shifts ( $\delta$ ): *anti-3*•[O], 53.5 ppm; *anti-3*, 32.5 ppm; *syn-3*, 19.0 ppm.

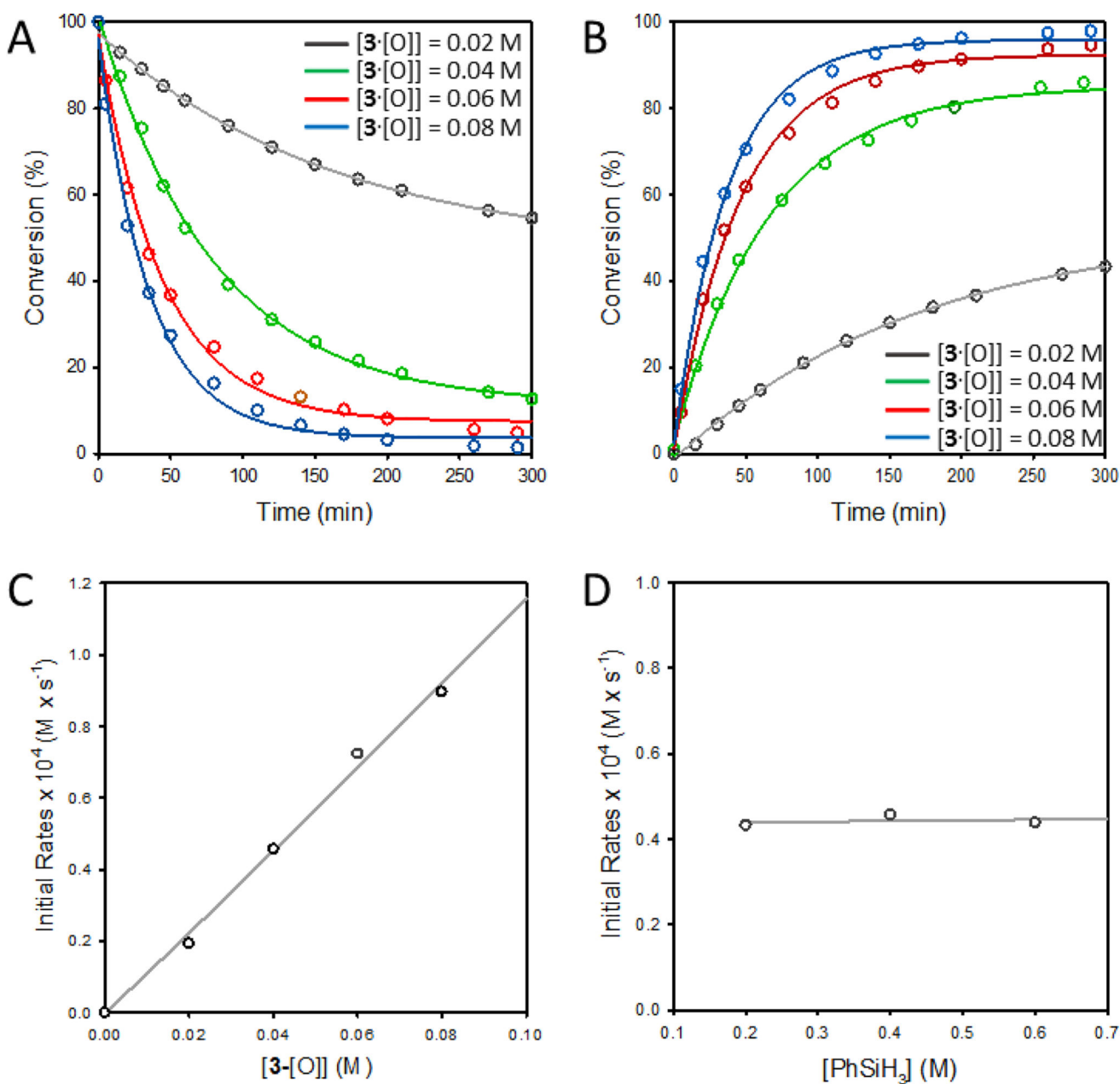


**Figure 3.** Kinetics experiments of catalytic reductive cyclization. (a) concentration of substrate  $\mathbf{1}$  vs time; (b) concentration of product  $\mathbf{2}$  vs time; (c) plot of initial rates of substrate  $\mathbf{1}$  consumption vs concentration of pre-catalyst  $\mathbf{3}\cdot\text{O}$ ; (d) plot of observed initial rates of substrate  $\mathbf{1}$  consumption vs phenylsilane concentration.

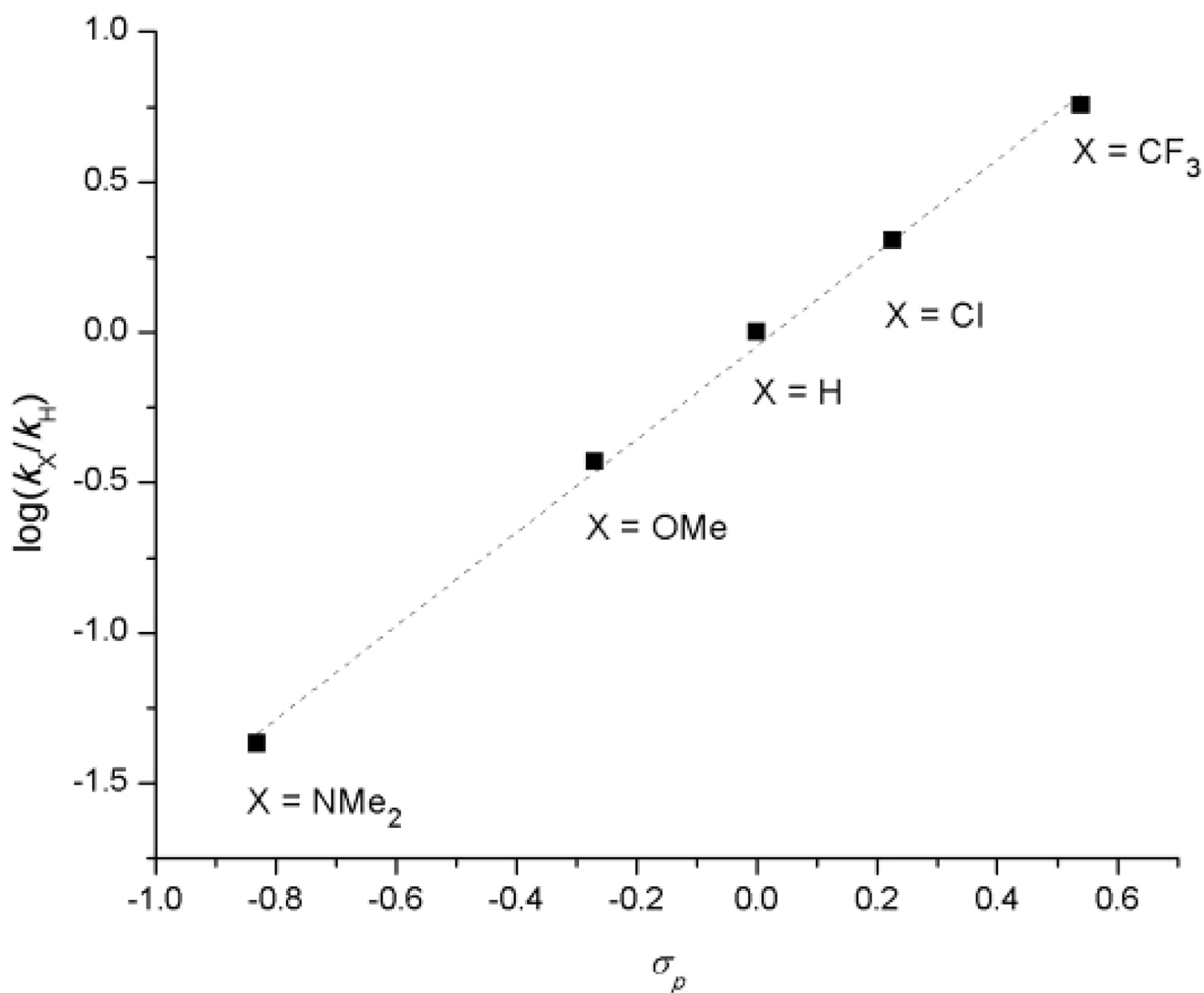


**Figure 4.** Hammett plot for carbazole formation mediated by 3 according to the reaction depicted in eq 3. Equation:  $y = 1.552x - 0.046$ ;  $R^2 = 0.9978$ .

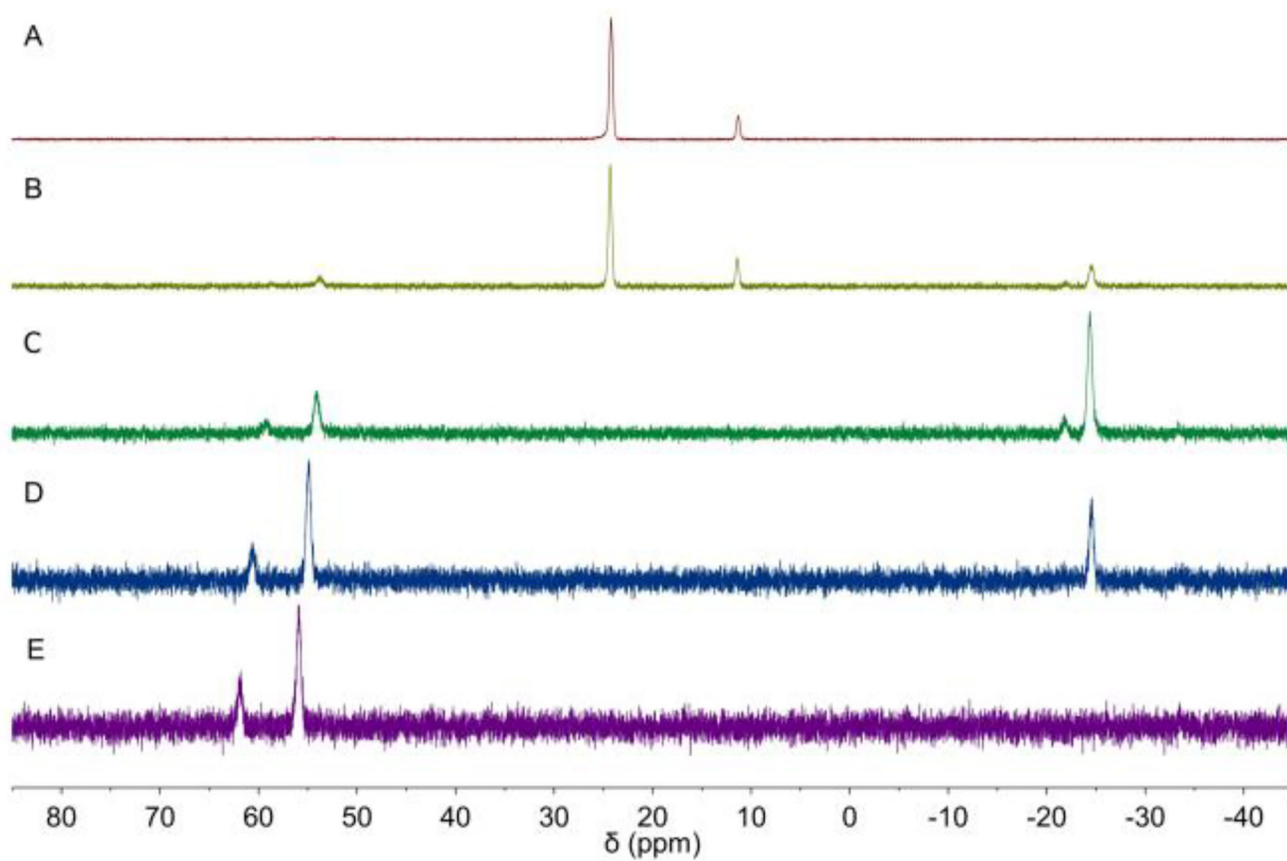


**Figure 5.** Time-stacked in situ  $^{31}\text{P}$  NMR spectra of the reaction of phosphetane **3** and 2-nitrosobiphenyl **28** ( $-60\text{ }^\circ\text{C} < T < -50\text{ }^\circ\text{C}$ , toluene- $d_8$ ). (A)  $t = 0$  min; (B)  $t = 120$  min; (C)  $t = 200$  min; (D)  $t = 300$  min; (E)  $t = 390$  min. Chemical shifts ( $\delta$ ): *anti*-**3**•[O], 54.1 ppm; *syn*-**3**•[O], 61.8 ppm; *anti*-**3**, 24.2 ppm; *syn*-**3**, 11.3 ppm; *syn*-**30**, -21.8 ppm; *anti*-**30**, -24.4 ppm.

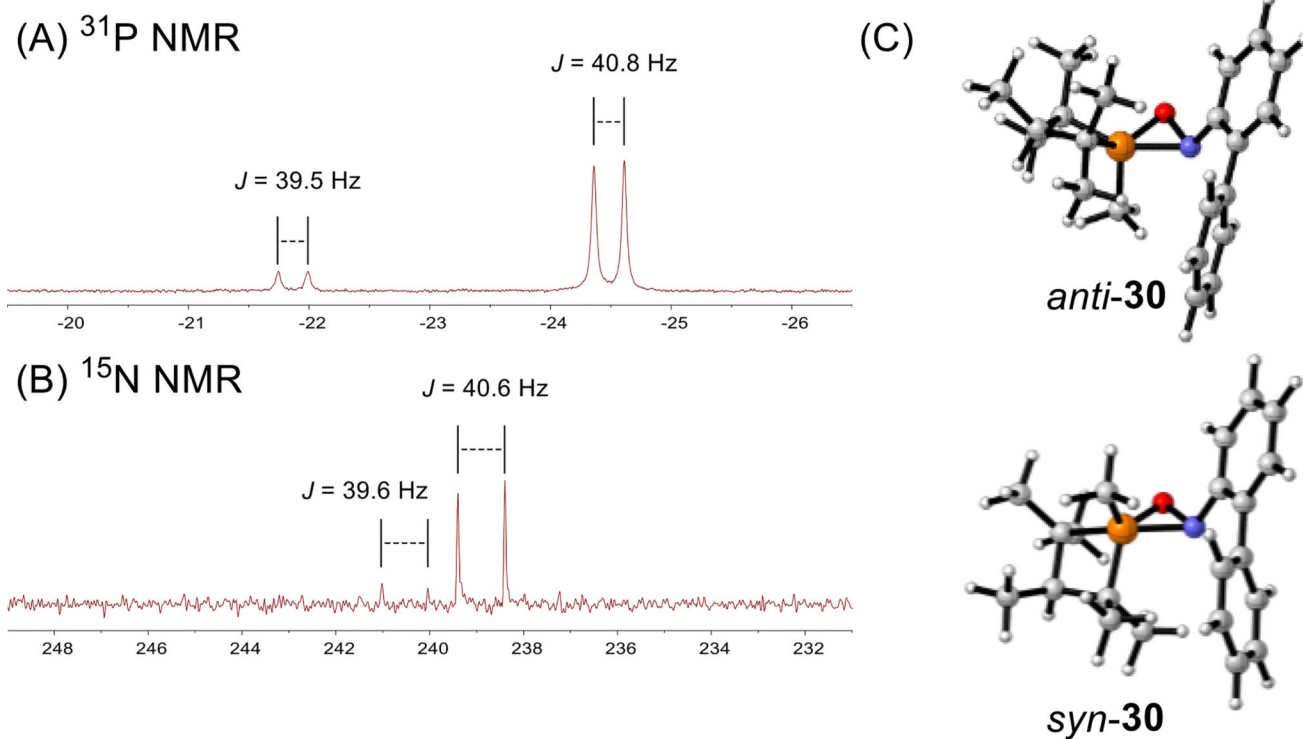


**Figure 6.** Heteronuclear NMR spectra of a reaction of phosphetane **3** and 2-( $^{15}\text{N}$ )nitrosobiphenyl **28** ( $-60\text{ }^\circ\text{C} < T < -50\text{ }^\circ\text{C}$ , toluene- $d_8$ ). Units are ppm relative to 85%  $\text{H}_3\text{PO}_4$  ( $^{31}\text{P}$ ,  $\delta = 0.0$  ppm) and liquid  $\text{NH}_3$  ( $^{15}\text{N}$ ,  $\delta = 0.0$  ppm). (A) Annotated  $^{31}\text{P}$  NMR spectrum. (B) Annotated  $^{15}\text{N}$  NMR spectrum. (C) DFT model of oxazaphosphiranes **30** ( $G_{\text{rel}} = -0.3$  kcal/mol favoring *anti-30*).

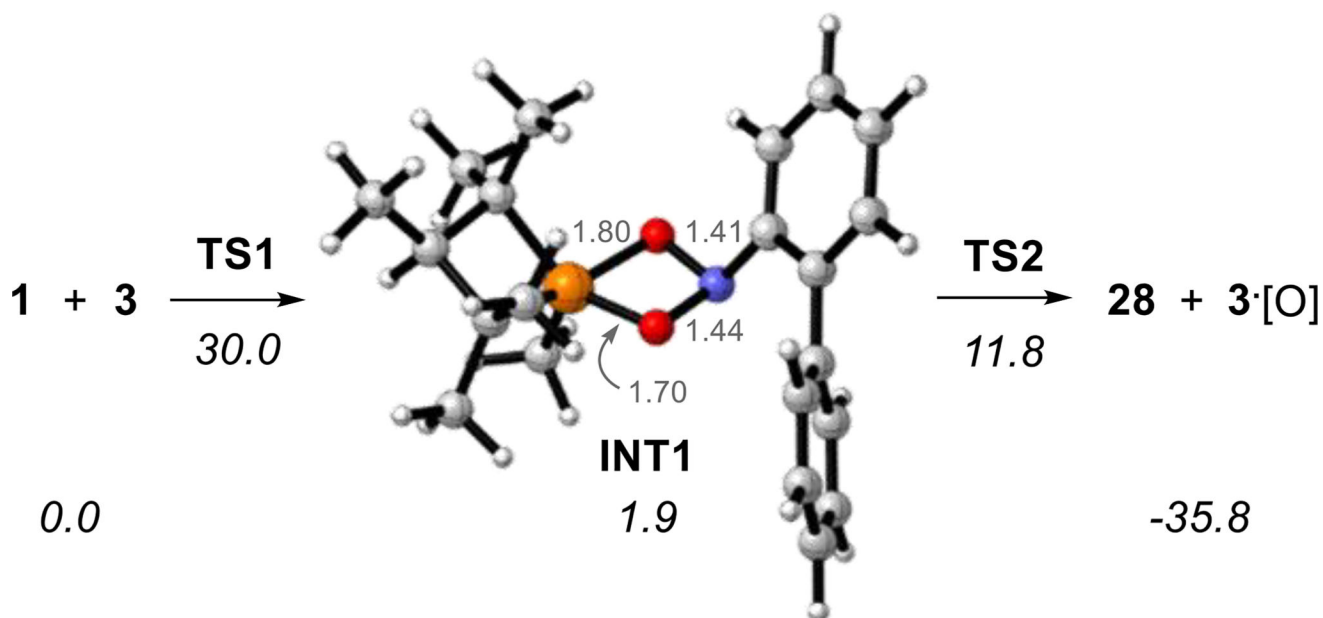


**Figure 7.** DFT mechanism (M06-2X/6-311++G(d,p)/PCM) for deoxygenation of 2-nitrophenyl **1** by phosphetane **3**. Relative free energies (kcal/mol) in italics. Phosphorus (orange), oxygen (red), nitrogen (blue), carbon (gray), hydrogen (white).



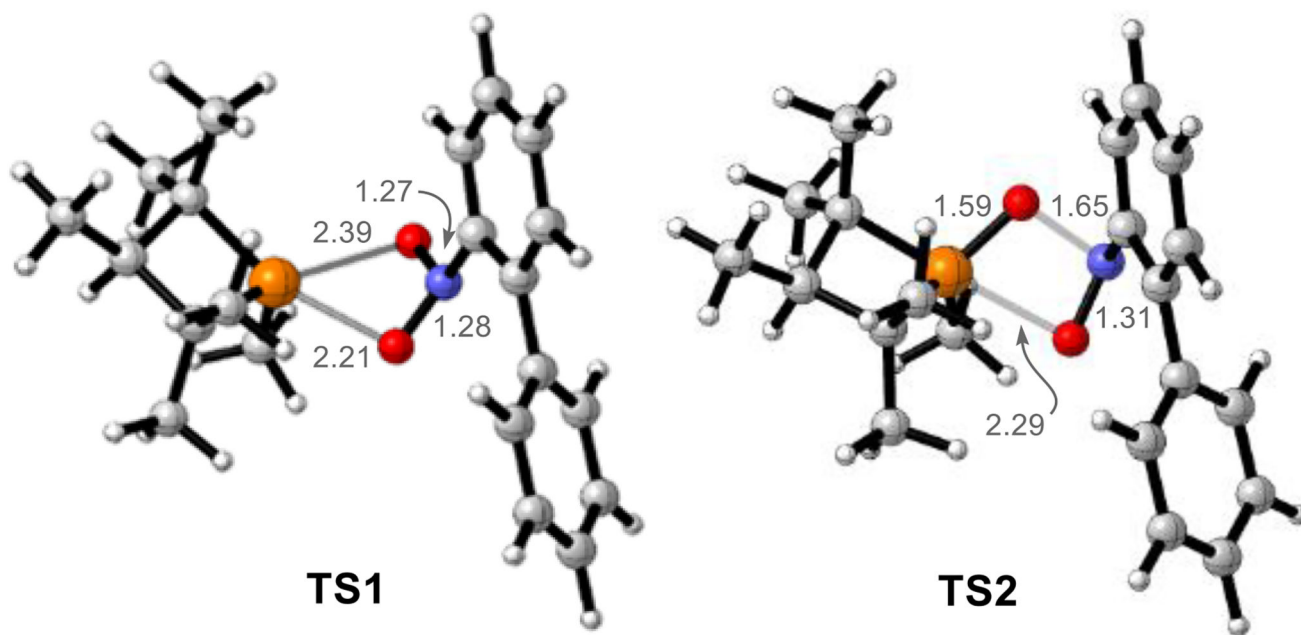


**Figure 8.** DFT transition structures (M06-2X/6-311++G(d,p)/PCM) along the stepwise deoxygenation pathway with selected bond metrics. Phosphorus (orange), oxygen (red), nitrogen (blue), carbon (gray), hydrogen (white).

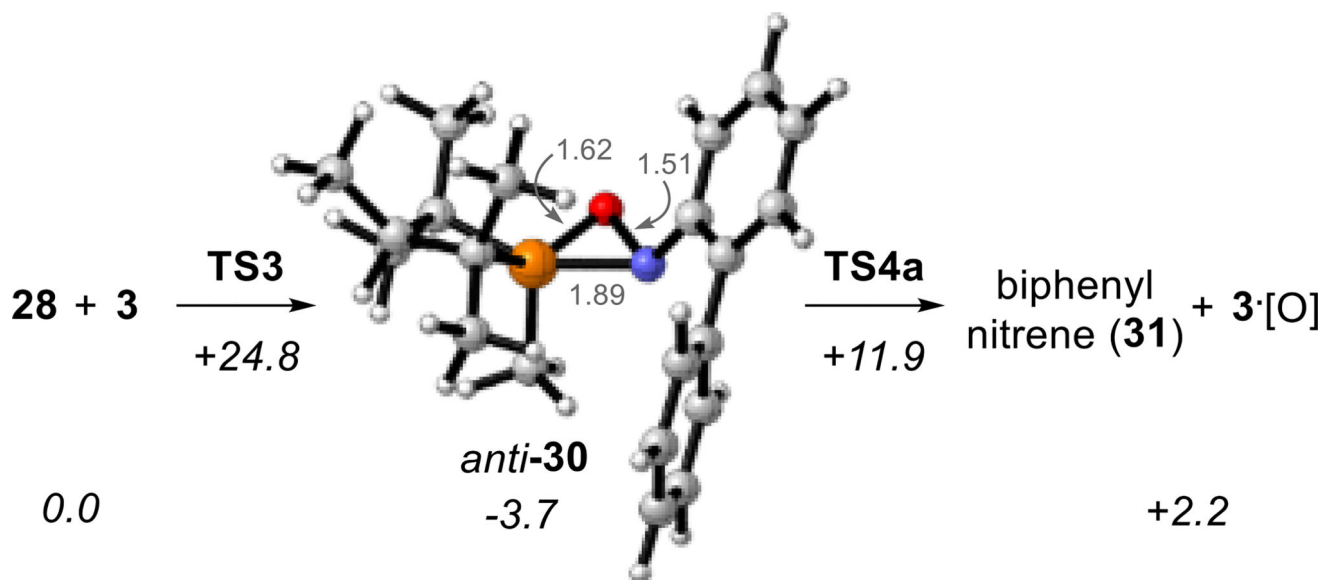


**Figure 9.** DFT mechanism (M06-2X/6-311++G(d,p)/PCM) for deoxygenation of 2-nitrosobiphenyl **28** by phosphetane **3**. Relative free energies (kcal/mol) shown in italics. Phosphorus (orange), oxygen (red), nitrogen (blue), carbon (gray), hydrogen (white).

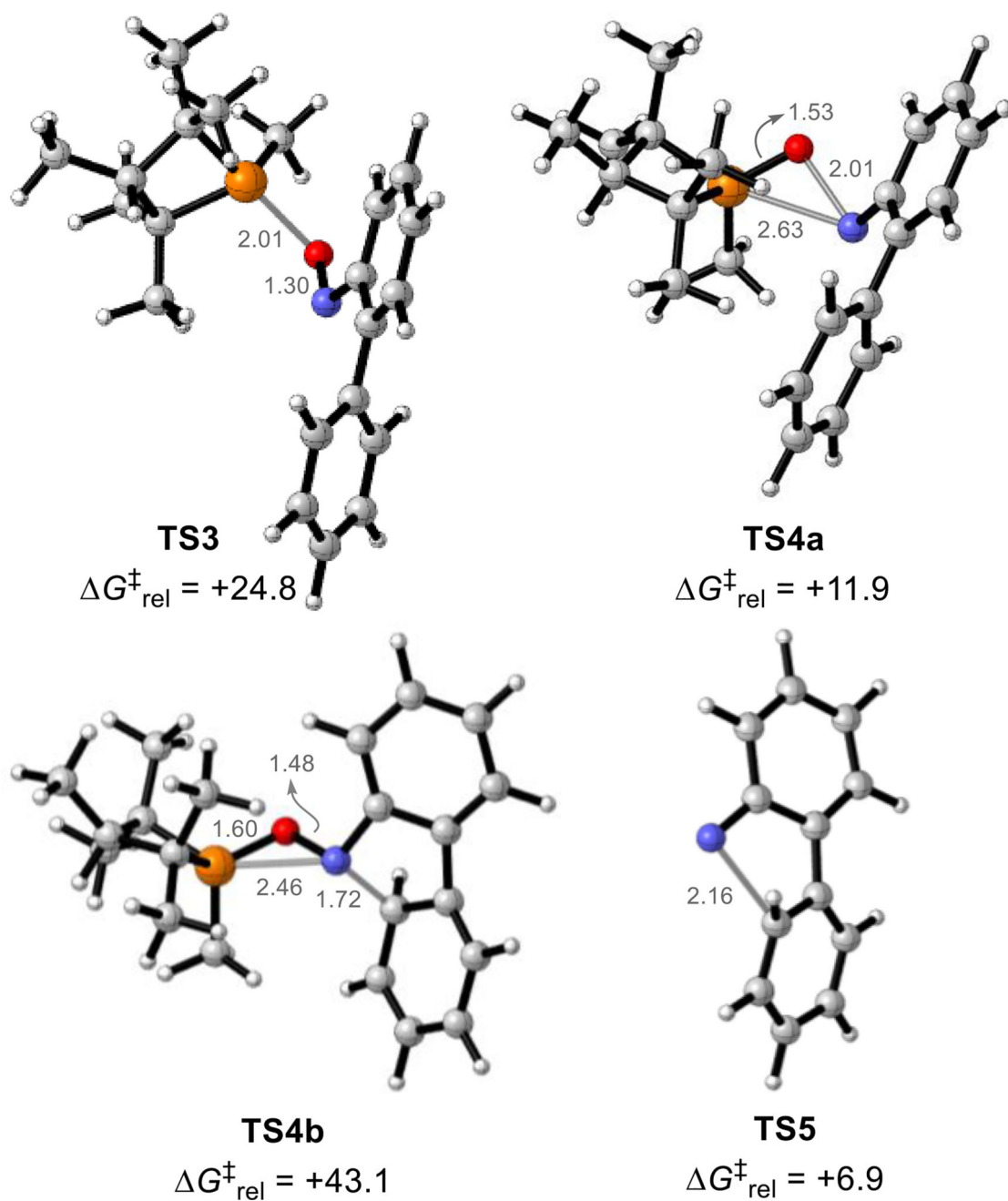


**Figure 10.** DFT transition structures (M06-2X/6-311++G(d,p)/PCM) along the stepwise deoxygenation pathway with selected bond metrics. Phosphorus (orange), oxygen (red), nitrogen (blue), carbon (gray), hydrogen (white).

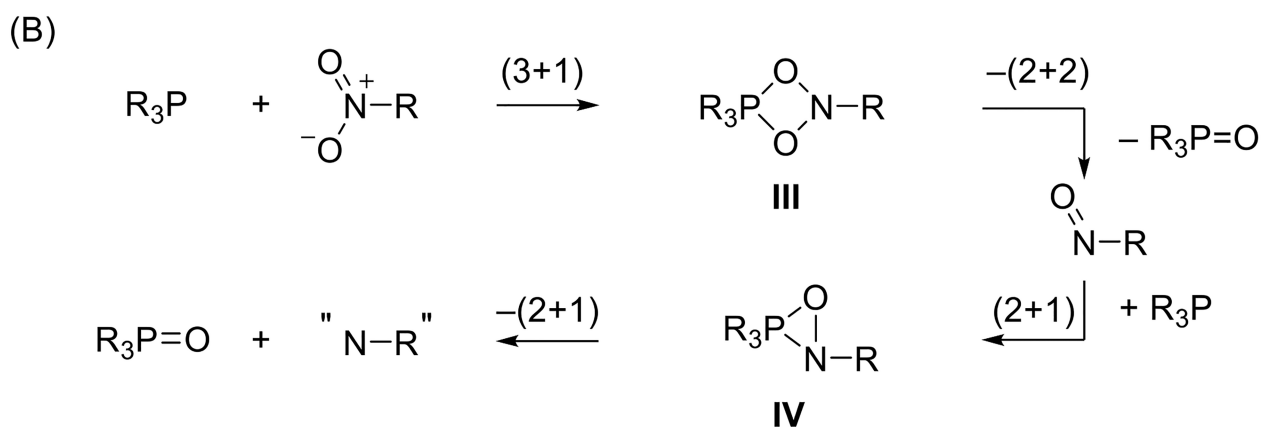
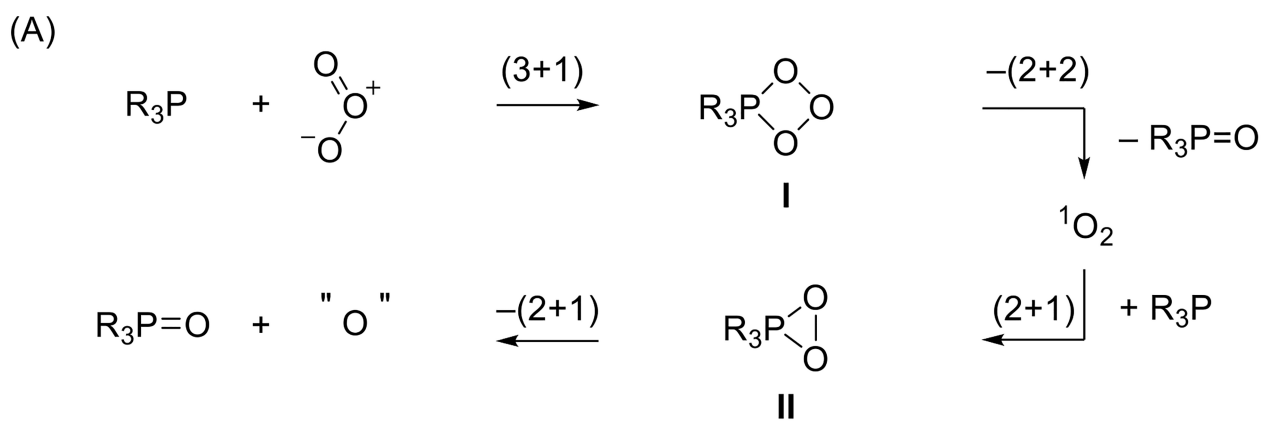


**Figure 11.**

Isolobal correspondence between (A)  $\text{O}_3$  and (B)  $\text{RNO}_2$  in their sequence of reactions with tricoordinate phosphorus compounds.



Table 2

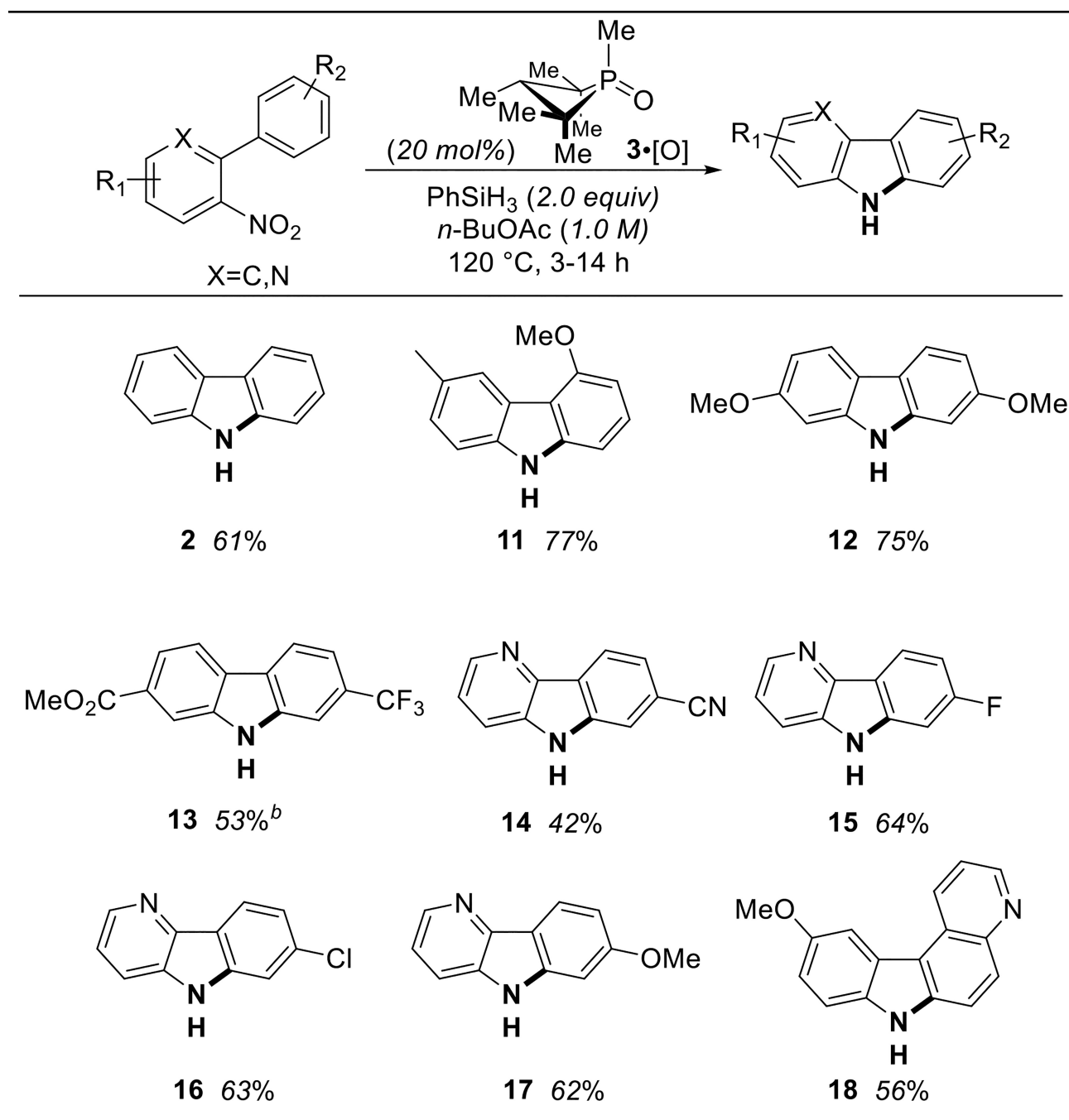
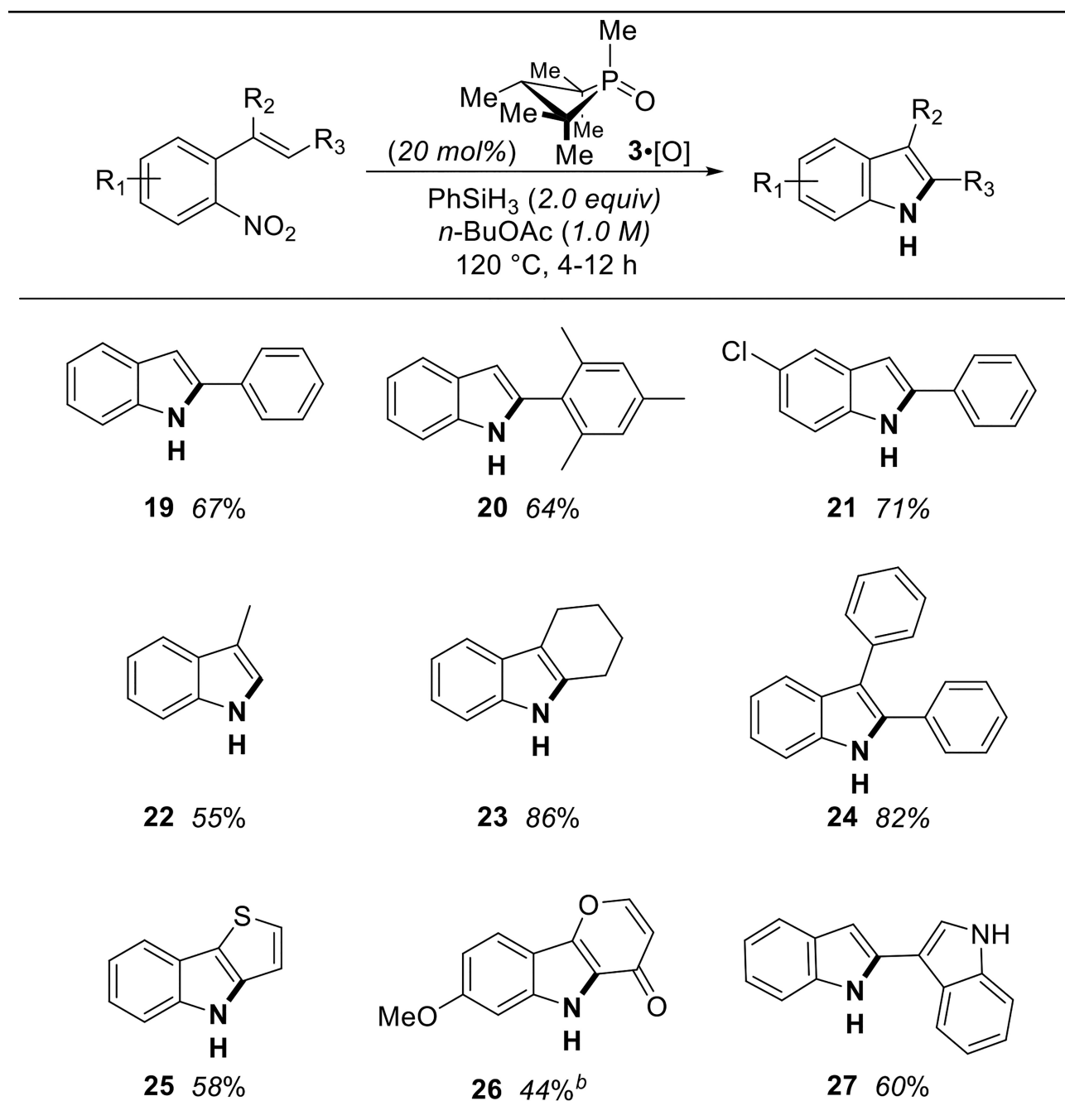
Examples of Catalytic Carbazole Synthesis.<sup>a</sup><sup>a</sup>Yields reported for isolated products.<sup>b</sup>(EtO)<sub>3</sub>SiH (4 equiv) was used as reductant. See Supporting Information for full experimental details.

Table 3

Examples of Catalytic Indole Synthesis.<sup>a</sup><sup>a</sup>Yields reported for isolated products.<sup>b</sup>Reaction was run on a half-gram scale. See Supporting Information for full experimental details.

**Table 4**Experimental<sup>a</sup> and calculated<sup>b</sup> <sup>31</sup>P NMR chemical shift values<sup>c</sup> for **3**, **3•[O]**, and **30**.

Compound	Chemical shift ( $\delta$ ) <sup>c</sup>	
	expt <sup>a</sup>	calc <sup>b</sup>
<i>syn</i> - <b>3</b>	+11.3	+14.3
<i>anti</i> - <b>3</b>	+24.2	+24.2
<i>syn</i> - <b>3•[O]</b>	+61.8	+52.0
<i>anti</i> - <b>3•[O]</b>	+54.1	+54.0
<i>syn</i> - <b>30</b>	-21.8	-28.8
<i>anti</i> - <b>30</b>	-24.4	-26.8

<sup>a</sup>Isotropic <sup>31</sup>P NMR (161.796 MHz) chemical shift in toluene-*dg* at  $T = -60$  °C.

<sup>b</sup>GIAO NMR chemical shift at the PBE1PBE/6-311G(2d,2p)//M06-2X/6-311++G(d,p) level of theory.

<sup>c</sup>Chemical shift ( $\delta$ ) in ppm referenced relative to 85% H<sub>3</sub>PO<sub>4</sub> standard ( $\delta = 0.0$  ppm).



**Table 5**

Experimental and computational linear free energy relationship correlation.

-X	$\sigma_{\text{para}}$	$k_{\text{X}}/k_{\text{H}}$		
		expt <sup>a</sup>	expt <sup>a</sup>	calc <sup>b</sup>
-NMe <sub>2</sub>	-0.83	0.04	+1.9	+2.8
-OMe	-0.27	0.37	+0.6	+0.5
-H	0	1.00	0.0	0.0
-Cl	0.23	2.01	-0.4	-1.9
-CF <sub>3</sub>	0.54	5.67	-1.0	-2.9

<sup>a</sup>See Supporting Information for full details.<sup>b</sup>Relative transition state free energy calculated by M06-2X/6-311++G(d,p).<sup>c</sup>Units are kcal/mol at T=298 K.